CRAWFORD, STEVEN, Ph.D. Cytotoxicity of Engineered Nanoparticles used in Industrial Processing. (2019)
Directed by Dr. James Ryan. 100 pp.

Engineered nanoparticles (NPs) are now heavily used in industrial processing where they are eliminated as waste after use. This waste is a mix of used nanoparticles and process byproducts. While research continues to be done on the toxicity of NPs due to size and composition of pristine material, waste NPs from industrial processes are likely to have modified properties that impact their level of toxicity. These studies investigate this transformation in physicochemical properties that has not been adequately explored by examining waste from relevant high-volume chemical mechanical planarization (CMP) processes used by the semiconductor industry. New (pristine) polish slurries and generated waste samples from various key CMP processes are fully characterized for relevant physicochemical properties to determine any transformation of NPs due to processing. Additionally, high throughput in vitro microplate-based assays assess the toxicity, oxidative stress, and mode of cell death for nanoparticles in both pristine and waste slurries to highlight any differences in biological effects. A combination of darkfield microscopy and inductively coupled plasma optical emission spectroscopy (ICP-OES) indicate cellular uptake of slurry nanoparticles. The results of this study explore the type, magnitude, and biological effect of transformed nanoparticles in CMP waste. The results presented support nanoparticle transformation as an important facet to consider in the risk assessment for new materials.

CYTOTOXICITY OF ENGINEERED NANOPARTICLES

USED IN INDUSTRIAL PROCESSING

by

Steven Crawford

A Dissertation Submitted to
the Faculty of The Graduate School at
The University of North Carolina at Greensboro
in Partial Fulfillment
of the Requirements for the Degree
Doctor of Philosophy

Greensboro
2019

Approved by

_____
Committee Chair

DEDICATION

To my wife Kelli and my family for helping me along the way.

APPROVAL PAGE

This dissertation written by Steven Crawford has been approved by the following committee of the Faculty of The Graduate School at the University of North Carolina at Greensboro.

Committee Chair_____

Committee Members_____

_____

_____

_____
Date of Acceptance by Committee

5/15/2019
Date of Final Oral Examination

TABLE OF CONTENTS

Page

LIST OF TABLES

Page

LIST OF FIGURES

Page

CHAPTER I

INTRODUCTION

Engineered nanoparticles (NPs) are synthesized and used for a wide variety of industrial and consumer products. Metals, metal oxide, and polymer nanoparticles can be found in products that come into direct contact with the general public, while others may enter the environment during synthesis or use. The global nanoparticle market has experienced growth over the past two decades in diverse fields such as aerospace, automotive, catalysts, coatings, paints, pigments, composites, cosmetics, electronics and optics, energy, filtration and purification, plastics, textiles and many others. To this end, approximately 300,000 metric tons of engineered nanomaterials were used just in 2010. While occupational exposure of researchers and engineers represent the first group at risk, most of these materials end up in landfills, the soil, or water. The growing prevalence and use of these various nanomaterials increase the average person's likelihood to be exposed to them over the course of one's life.

I.1 The Effect of Industrial Processing on Engineered Nanoparticles

In the growing global market for engineered nanoparticles, electronic applications in the semiconductor industry make up the lion's share at well over $1 billion annually. For the last decade, the largest segment has been polishing slurries for chemical-

mechanical planarization (CMP). Silicon oxide, cerium (IV) oxide and aluminum oxide nanoparticles are among those most commonly used by modern processing techniques. [1] The CMP process uses massive quantities of these nanoparticles in a slurry form to polish and planarize wafers via some ratio of both chemical interaction and/or tribo-mechanical removal of material. [38] As material is removed from wafers, it is mixed with the used slurry and rinse water and then discharged after varying degrees of treatment or reclamation depending on the region. [7,37] Tens of liters of waste slurry is generated each wafer polish cycle, and 40% of all water used in the manufacture of integrated circuits is consumed by CMP. [2, 9, 22]

Huge quantities of nanoparticles are used in slurries so wastewater from the CMP process can pose a health hazard by the pollution of water systems and soil with these engineered nanoparticles. [25, 47, 55] In addition to any intrinsic toxicity of the bulk materials, nanoparticles can be more toxic due to their high surface area and ability to penetrate biological membranes. [15, 33, 34] Due to the mixed chemical and mechanical nature of the CMP process, the slurry nanoparticles may also become impregnated or bound to lesser amounts of the removed substrate material, further complicating and potentially increasing the toxicity of the mixture. [3] Although the toxicity profile of many of the pure materials used in the process have been investigated, the effect of mixing potentially transformed nanoparticles with removed substrate material is poorly understood and has not been researched adequately. [3, 5, 6, 11, 14, 19, 20, 23, 24, 31, 32, 36]

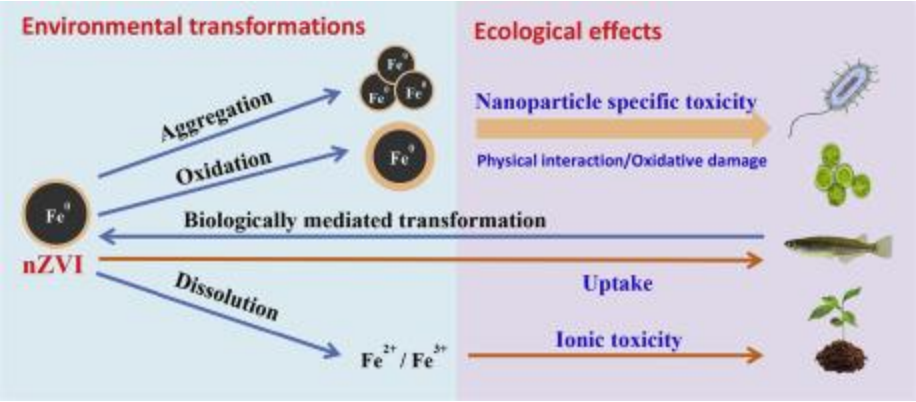

Figure 1.1 Transformation and Effect of Nanoparticles in the Environment. [53]

Previous studies and existing literature pertaining to the toxicity of CMP waste have not adequately characterized physicochemical properties to assess any transformation or modification to the engineered nanoparticles resulting from the process. [29] The toxicity profiles of nanomaterials can vary tremendously based on size, surface area, surface chemistry, and many other properties, even with nanoparticles of similar chemical composition. [13, 15, 16, 17] Understanding the hazards of only the newly manufactured, pristine nanomaterials is not sufficient for the regulation of transformed waste that is discharged in a modified form. Waste needs to be investigated for toxicity in comparison to its original pristine form to determine the biological effect of physicochemical changes. To make sense of the complicated landscape of nanoparticle health and safety, any changes in toxicity need to be tracked, studied, and attributed to the physicochemical property changes that can result from industrial processing. [29] This information will enable the development of new methods for evaluating the health and safety impacts of new processes or materials with an emphasis on green engineering.

I.2 Hypothesis and Goals

This dissertation details the work undertaken to explore the science behind process-related nanoparticle transformation and its effect on mammalian cells. The hypothesis that motivated this research is that **in industrial processes that use NPs such as CMP, waste NPs are likely to modify/transform physicochemical properties of those NPs, which may result in altered toxicity and associated hazards.** Specifically, this research sought to establish that A) CMP slurry NPs will be transformed by the CMP process and B) those transformed NPs will cause a discernible difference in cellular toxicity.

To test the hypothesis, specific aims and objectives were established:

1) **Specific Aim:** Assess the transformation of nanoparticles in common slurry types from a representative group of CMP polish processes.
    a. Objective 1.1: Generate and characterize physicochemical properties of pristine and waste slurry samples to assess transformation of NPs.
2) **Specific Aim:** Compare pre- and post-process nanoparticles for effect on cell viability, mode of cell death, and oxidative stress in lung, liver, and macrophage cells.
    a. Objective 2.1: Determine dose-response for cell viability.
    b. Objective 2.2: Determine mode of cell death and ROS generation level
3) **Specific Aim:** Assess any differences in the amount of nanoparticle uptake and localization for transformed nanoparticles versus pristine.
    a. Objective 3.1: Determination of total nanoparticle uptake by ICP-OES

b. Objective 3.2: Darkfield imaging to determine localization

In the completion of these aims and objectives, relevant off-the-shelf CMP slurries and common *in vitro* immortalized cell lines were used. All process and slurry combinations were characterized and used for toxicity studies, regardless of detectable transformation in properties. Additional objectives specific to one process, GaAs polishing, were also added and explored. Due to the unique results of this process, it is explored on its own in Chapter V.

CHAPTER II

REVIEW OF THE LITERATURE

II.1 Unique Toxicity of Nanoparticles

Nanoparticles and other nanomaterials have distinct toxic effects from bulk material or molecular forms. Over the past two decades, research has shown that the unique physicochemical characteristics of nanomaterials are the reason for their unique toxicology. Increased surface area with small size compared to other particulate toxicants, unique surface groups and structure, coatings, and aggregating properties have all been shown to play a role in toxicity. Regardless of chemistry, nanomaterials can play a role in the biological machinery at cellular and subcellular levels. At the lowest end of the nanoscale range, many materials diffuse easily through all membranes and permeate through all structures of the cell and tissue. [25, 29]

At the nanoscale, even metals such as gold can become highly reactive. Very specific size ranges can lead to finely tuned properties. Known toxic thresholds for molecular forms can be orders of magnitude higher or lower for nanoparticle variants. Though born from ultrafine particle toxicology, nanotoxicology distinguishes itself as a sub-specialty where classic toxicity rules may not always apply; new insight and methods of study are required to elucidate the biological effect of these new materials. Once the research established that nanomaterials distinguished themselves from standard materials in toxicology, nanotoxicology has become an established sub-specialty of toxicology.

Safety and toxicity of nanomaterials is an important field of study. Furthering the scientific community's understanding of nano-related environmental health and safety will also help governments and industry regulate a rapidly growing class of materials. Nanoparticles should not be regulated at the same levels as traditional materials due to the shift in toxicity for many materials. In addition to the study of their varied toxic effects, nanomaterials must also be carefully characterized so that toxicity and physicochemical properties may be correlated. [29]

II.2 The Effect of Physicochemical Characteristics

The unique toxicity of engineered nanomaterials comes from specific properties, both physical and chemical. Size, surface area, morphology, chemical composition, surface groups, and charge are among those that play a major role in nano-bio interactions. No single property can be pinpointed to a given toxic effect, but an overall characterization of nanomaterials can indicate the potential for toxic effects. As more research is done, the potential to correlate toxicity with specific physicochemical characteristics grows.

Nanoparticle size is the most obvious property to influence toxicity. [72] As a nanoparticle decreases in size, its effective surface area per mass increases. Decreased size means cells can more readily uptake NPs; increased surface area means greater reactivity with any surface chemistry on the NP. The combination of these two effects has the potential to greatly alter the behavior of tissues compared to larger particles. NPs have been shown to induce inflammation and oxidative stress (reactive oxygen species, ROS) in many cell and tissue types. Most NPs demonstrate a size- and dose-dependent

toxicity, typically with smaller particles causing the greater effect. For NPs whose surface chemistry plays a role in ROS generation, greater surface area due to smaller size increases the ROS capacity.

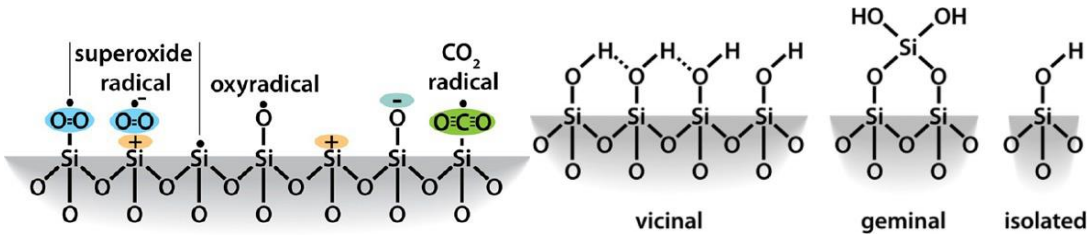

Figure 2.1 Radicals and Silanol Groups that can Exist on an Amorphous Silica Surface. [16]

II.3 Amorphous Silica Nanoparticles

II.3.1 A common material

Among engineered nanomaterials, Silica (SiO_2) NPs are one of the dominant materials used. Silicon is the second most abundant element on earth, so silica is incredibly inexpensive, in addition to being easy to prepare and relatively biocompatible compared to other materials. The ease of surface functionalization of silica particles means they can also be used for a wide range of applications. [57] Silica comes in many forms, all of them useful for one application or another. The multiple crystalline forms of silica are the most well-studied for health effects, causing silicosis and other severe respiratory disease, but it is not as commonly used for ENMs. The most commonly used by far is amorphous silica. Amorphous silica itself has two distinct types; fumed (or pyrolytic) that is dry formed in a furnace, and colloidal silica (Stöber silica) which is formed at low temperature in water. Colloidal silica, also called mesoporous silica, has

growing interest behind it for biomedical purposes due to the higher surface areas and porous interiors that help facilitate the encapsulation of hydrophobic therapeutic drugs for delivery within the body. Functionalization also allows its use in selective and ultrasensitive biosensors, immunoassays, labelling, imaging, and cell targeting. [76, 77] In industry, amorphous silica is used as catalysts, desiccants, abrasives, and fillers to tune mechanical properties. Amorphous silica is the most abundant of any currently used nanoparticle. [16] Despite being classified as "generally considered safe" by the FDA, the lack of long-range order in amorphous silica and its wide range of commercially used sizes, porosities, and functional groups, specific toxicological behaviors are not well understood now.

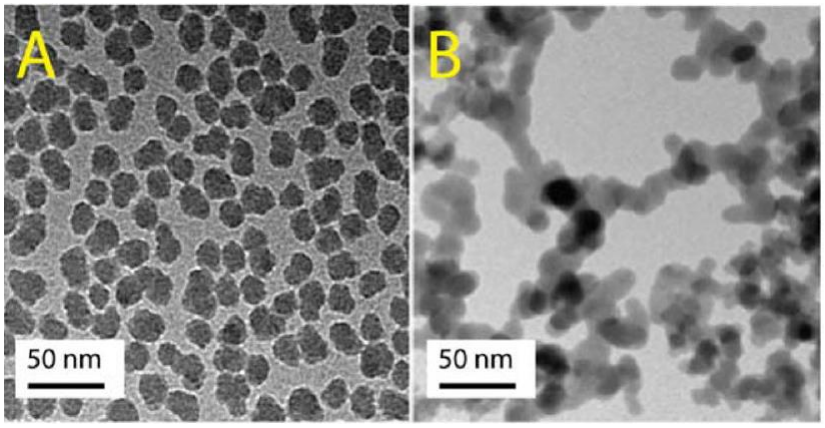

Figure 2.2 Representative TEM Images of Round Colloidal Silica NPs (A) and Chain-like Aggregation of Fumed Silica NPs (B). [16]

A key element for determining toxicity of amorphous silica is an understanding of the expected variability amongst NPs. Because surface chemistry, shape, porosity, and size are tunable elements of SiNPs and important factors in toxicity, it is vital that proper

characterization be done for particles when a toxicity study is conducted. Only by correlating physicochemical characteristics with variabilities in biological effects amongst SiNPs may a true understanding of toxicity be attained. Due to the increased surface area of NPs, potential surface groups are a major item of interest. Variable silanol groups or radicals can exist on the surface of the particles and inside pores (figure 2.1). [16]

Notable among existing literature on silica toxicity is the variability in results. For example, some groups report no change in toxicity with varying size, while others show a sharply size-dependent effect. [34, 60] It is imperative that variations in particle chemistry, cell type, and route of exposure be considered when drawing conclusions on toxicity data from various studies. One of the most common uses for amorphous silica NPs is as an abrasive in the electronics manufacturing industry for a process called Chemical Mechanical Planarization. Due to the nature of these abrasives (slurries), there are frequently surface modifications and the addition of proprietary materials that make for complex mixtures that are more difficult to study. [5, 65, 71]

In many cases, occupational and public exposure to amorphous SiNPs is in an aerosolized form. [5] For this reason, many studies use similar protocols to that of studying ultrafine particle toxicity; lung epithelial cells and macrophages are most commonly used. Red blood cells are also common as some SiNPs have been shown to cause hemolysis. [23, 62, 64, 66] Other commonly used cell lines specific to other routes of exposure have also been used: keratinocytes for dermal exposure and hepatic cells for particles that are absorbed in the body among others. [60, 63]. Many current studies

have been *in Vitro* with limited animal studies published on the systemic mechanism of amorphous silica. Varying metabolisms and ROS susceptibility lead to similarly varying toxicity levels. [73]

II.3.2 Uptake and internalization

In higher concentrations, it has been shown that aerosolized NPs appear in many parts of the body and can cause toxicity in the liver, heart, and nervous system. Studies using marked polystyrene beads have been conducted to mimic metal oxide NPs. Data indicates NPs enter every compartment of the lung and become localized within epithelial, endothelial, fibroblast, and even red blood cells. This study also showed that particle distribution across the lung were proportional to their relative volume and distribution did not appear selective. Among macrophages, particles of many sizes were phagocytosed, with concentrations inversely proportional to their size. In non-phagocytosing cells, only the smallest particles (NPs) are internalized. [72]

Particles up to 500nm have shown higher association with macrophages and phagocytic cells than epithelial and other non-phagocytic cells. Particles <100nm are taken up much faster and at higher levels in lung macrophages versus epithelial cells. [62] In another study, spherical colloidal SiNPs showed that they were more likely to be taken up by BEAS-2B and THP-1 cells, whereas the more elongated fumed silica particles aggregated along the outer cell membrane. [16] An in-depth study using hepatic cells suggest that SiNPs can enter the cell by endocytosis and through membrane damage; other studies suggest this may be size and surface dependent. [63] SiNPs have been shown to be internalized in the cytoplasm and colocalized with lysosomes and

endosomes of each cell type studied so far, with none present in the nucleus. Concentrated particles at endosomes and lysosomes with evenly spread particles throughout the nucleus indicate that there are multiple uptake routes, or the particles are escaping from the endosomes/lysosomes over time. [62] TEM imaging done by various groups indicate that internalized SiNPs do not show any change in size or shape. [16,72]

A study on the uptake of SiNPs with and without a preformed protein corona demonstrated bare particles are more readily internalized to the cell. Those particles covered with a protein corona from biological fluids were not as efficiently taken up. The corona-free particles accumulated in lysosomes and freely in the cytosol, whereas corona-coated SiNPs were localized in lysosomes only.

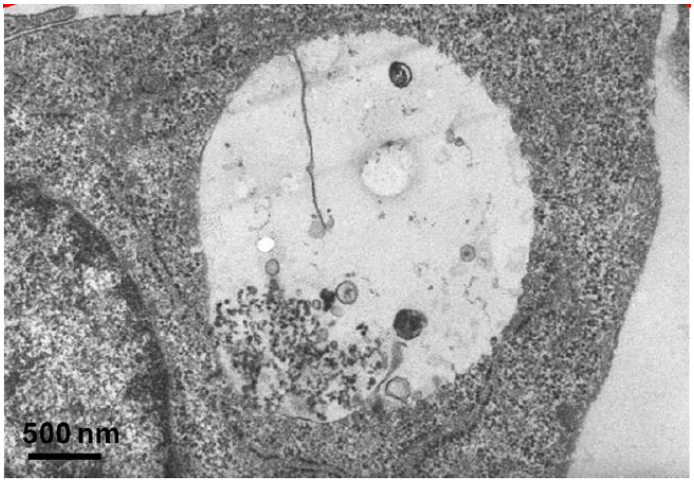

Figure 2.3 Colloidal Silica NPs Internalized in an Endosome. [16]

II.3.3 Membrane integrity

As discussed, one route of uptake for SiNPs involves the damage of the cell membrane. This seems to be more evident in smaller particles, and cells with lower

metabolic rates seem to be more susceptible than tumor cell lines. [73] In many studies, this membrane damage, typically determined by LDH release, also correlates with a proportional drop in cell viability, causing toxicity near 50 ug/mL SiNPs depending on the cell line. Interestingly, the study with keratinocytes show no loss of membrane integrity with particles >100nm, despite the loss of viability (below). This suggests that while membrane damage contributes to the toxicity of SiNPs based on the available specific surface area of the particles (reducing size), it is not the sole source of toxicity. For that study, there was no apparent ROS generated which may be based on the chosen cell type. [60] A similar size-dependent trend was also demonstrated using 21nm and 48nm SiNPs in myocardial cells, as well as 46nm and 64nm SiNPs in hepatic cells. [61,63] Size-dependent toxicity is a trend common in many types of nanoparticles but especially with regards to membrane integrity. In many cases, higher LDH levels also correlated with irregular morphology, cellular debris, and nuclear condensation, suggesting necrosis had been induced. In most cases, membrane integrity has correlated with increased ROS production and loss of viability. [23]

Contrary to these results, some studies using phagocytic cells (macrophages) do not show a clear size dependency for membrane damage, and in some cases the larger particles can cause more damage than particles <100nm. This same study also showed that surface functionalized particles induced less damage than plain particles, but it did not matter what the surface functionalization was (Amine and Carboxyl groups tested). [62]

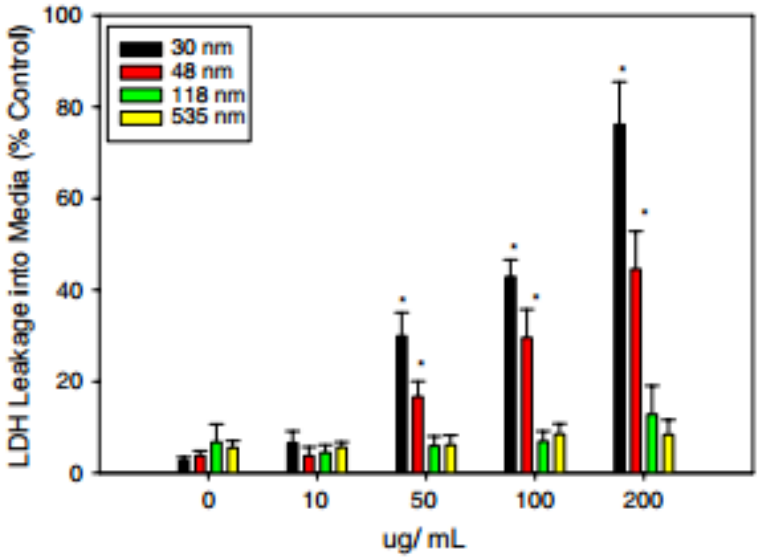

Figure 2.4 LDH Release Profile Indicating Membrane Damage for Smaller Silica NPs. [60]

II.3.4 Reactive oxygen species

Nearly every study on the toxicity of NPs has discussed a size-dependent inverse correlation with ROS production and viability. Reactive oxygen species formation, GSH reduction, or MDA levels (lipid peroxidation) were tested in nearly every study listed in this review. The smallest SiNPs were the only ones to show significant change for many. Increased ROS generation is an indicator for oxidative stress, MDA levels are the end products of lipid peroxidation, and GSH is a ubiquitous molecule that maintains redox homeostasis; each were affected in a dose dependent and inverse size dependent manner for SiNPs. Some studies also indicated that SOD and GSH-PX activity was significantly decreased, showing an inhibition of antioxidant capability in cells. MDA levels sharply increased for very small SiNPs (<50nm) while larger particles showed a more gradual

increase. These trends were demonstrated and correlated strongly with reduced viability in macrophages as well as cells from the kidney, lung, skin, and liver. [23, 60, 62, 64, 67]

The trends in ROS damage closely mimic the general trends of other NPs and ultrafine particles; higher levels of ROS production correlate strongly with cell death, particularly necrosis. However, the prevalence of observed toxicity even without ROS indicates that there are multiple mechanisms influencing toxicity as with membrane damage.

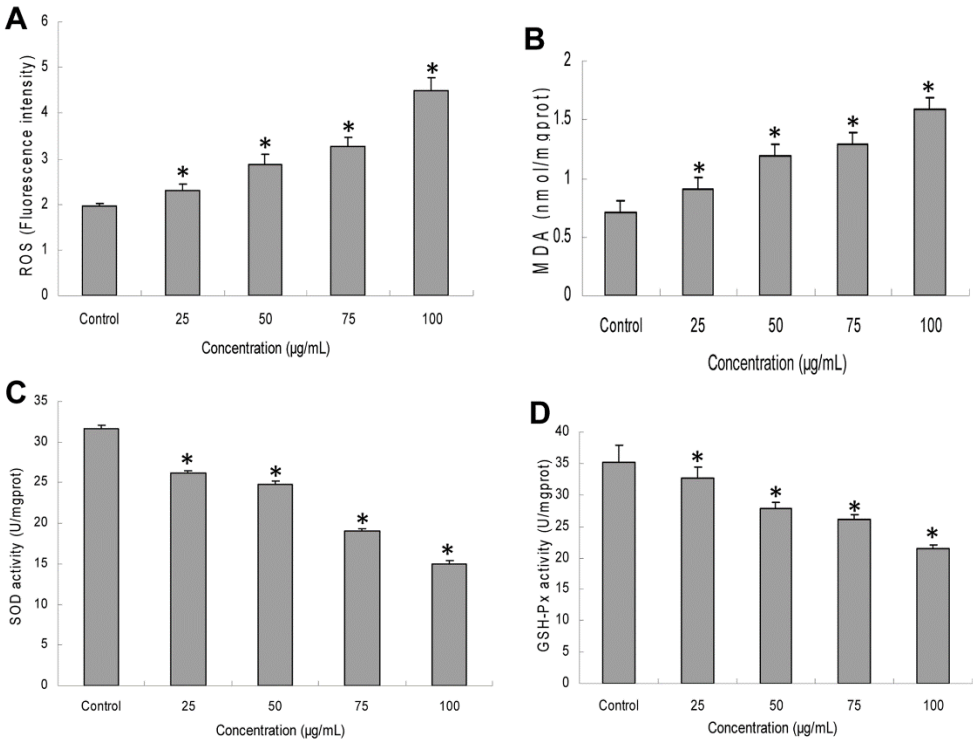

Figure 2.5 Typical Trends for ROS, MDA, SOD, and GSH-Px that are Concentration Dependent. Effects tend to increase with decreasing size.

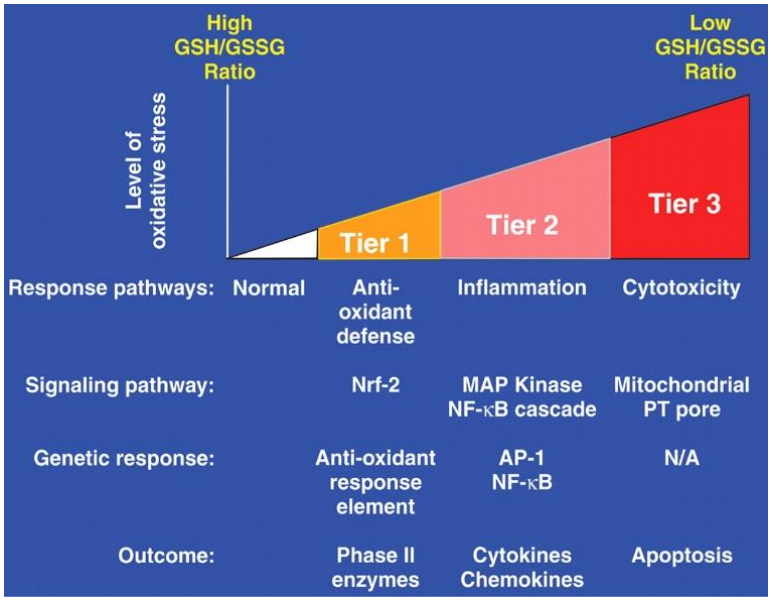

Figure 2.6 Hierarchical Oxidative Stress Model. [26]

II.3.5 Mode of death and cell cycle analysis

It has been shown that SiNPs can reduce cell viability in a dose-and size-dependent manner. Recent studies have investigated the mode of cell death for certain particle variations. Cell death is typically split into apoptosis (or autophagy) and necrosis for the sake of many studies. Apoptosis is the primary method of programmed cell death and does not involve membrane damage. Necrosis leads to membrane disruption and the leaking of cell contents. In most studies, necrosis was the dominant mode of death that correlated strongly with membrane damage and was concentration and size dependent. Apoptosis was also induced, but to a much lower extent. [63, 68] When surface modified SiNPs were tested, however, apoptosis was the primary mode of death, regardless of the specific functional group. These cells also had higher overall viability rates versus their bare counterparts. [10, 62]

Genotoxic studies have not demonstrated any evidence of genotoxicity from colloidal SiNPs on fibroblasts and endothelial cells except at elevated concentrations when cells become necrotic. There has been no discernable genotoxicity measured regardless of SiNP size for macrophages or epithelial cells. However, there are significantly fewer studies regarding direct genotoxicity compared to fumed and crystalline SiNPs, so this should be further explored. [70, 74]

Cell cycle analysis has been conducted by some groups. This type of analysis can quantify the number of cells in the G_0/G_1, S, and G_2/M phases. Cell cycle anomalies are often an indication of cell or DNA damage. It has been shown in certain cell types that the cell cycle is arrested in the G2/M phase following SiNP exposure to HUVEC (human umbilical vein endothelial cells). Similar studies using macrophages and epithelial cells showed no change. [62] The ratio of G2/M cells increase in a dose-dependent manner with S and G0/G1 cells sharply declining. The cell cycle arrest correlates with the same particles and dosages that exhibit high ROS so it is suggested that oxidative DNA damage may cause the G2/M arrest. G2/M plays an important part in mitosis and the arrest may be an attempt by cells to allow more time to repair DNA damage. When the damage is more than be repaired, apoptosis occurs. The molecular pathways for these effects are not yet fully explored. SiNP exposure triggers DDR pathways by suppressing Cdc25C, Cdc2 and cyclin B1 and sharply upregulating Chk1, which is typically activated in response to DNA damage, particularly as it pertains to the G2/M damage checkpoint signal transduction pathway. It was hypothesized that ROS generated by SiNPs cause oxidative damage to DNA, triggering the upregulation of Chk1 which inhibits the

downstream target of Cdc25c, which in turn downregulates cyclinB1/Cdc2 kinase, which is required for cells to enter mitosis. When Cdc2 is inactive and unable to bind cyclin B1, the G2/M transition cannot occur. This mechanism for SiNPs has not yet been corroborated by other literature. [68]

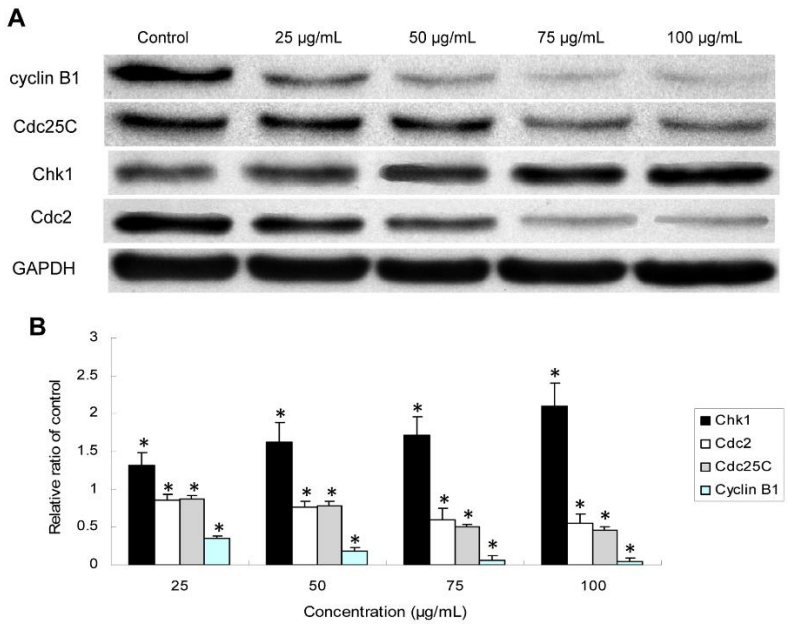

Figure 2.7 The Effect of Silica NPs on G2/M DNA Damage Checkpoint Signaling Pathway (Proposed Mechanism). [68]

Hemolytic activity is often a concern for SiNPs in general due to existing data on hemolysis by crystalline silica particles. Further research has shown considerable potential for hemolysis for fumed SiNPs, but very little hemolytic activity up to 200 ug/mL for colloidal (Stöber) SiNPs. [16]

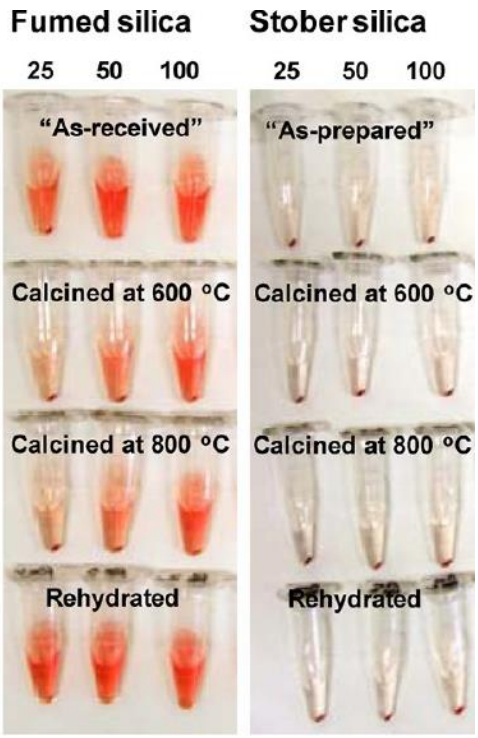

Figure 2.8 Hemolysis Caused by Fumed Silica, Not Colloidal Silica NPs. [16]

Additional pathways and markers have been explored by certain groups. Earlier studies linked the involvement of IL-1β production with the pathogenesis of pulmonary fibrosis possibly activating the Nalp3 inflammasome. Other targets in the pathway such as Cathepsin B release were also studied, but colloidal silica SiNPs did not have any effect. Fumed SiNPs increased IL-1β production in a dose-dependent manner. [16]

Gene set enrichment analysis provides a snapshot of overall cell processes and their changes in response to a stressor. GSE on 10nm and 500nm colloidal SiNPs indicate dosed cells indicate seven major pathways affected by the particles. Transcription regulation, cell cycle regulation, and inflammatory response were affected by both sizes. Apoptosis, differentiation, and signal transduction were affected only by

the 500nm particles and anatomical structure morphogenesis only by the 10nm particle. When compared to one another, the upregulations were not quite statistically enriched ($p<0.05$) and no clear transcriptional changes took place to the gene changes. The only process to rise above significance for the small particles was Nr4a2, an orphan nuclear receptor that promotes inflammation in activated macrophages and Egr2, an early response gene commonly induced in macrophages exposed to fibrous particles. For the larger particles, the cation transport process was upregulated. These genes include those involved in regulating metal transport. [34, 58, 59, 69]

II.4 Nanoparticle Transformation

Nanoparticles and other engineered nanomaterials are significant from an environmental health and safety perspective as detailed thus far. As with other toxicants of interest, ENMs are characterized and tested for toxicity *in vitro* and *in vivo* to determine their various biological effects and establish suggested exposure limits. Nanomaterials that are used or in incorporated in consumer products inevitably enter the environment, contaminating the air, soil, and water as other materials do. Sunscreens, tires, sporting equipment, electronics, lubricants, cleaners, and filtration are among the ever-growing list of products using nanomaterials. As the nanoparticles are incorporated into a product, they can change slightly from their original form, and change further still as the product ages or weathers. ENMs used in the production of products, such as in the electronics industry, can also change form after being used. ENMs can also be transformed once they have entered the environment as well, reacting with or being shaped by external forces. [41, 42, 43, 57]

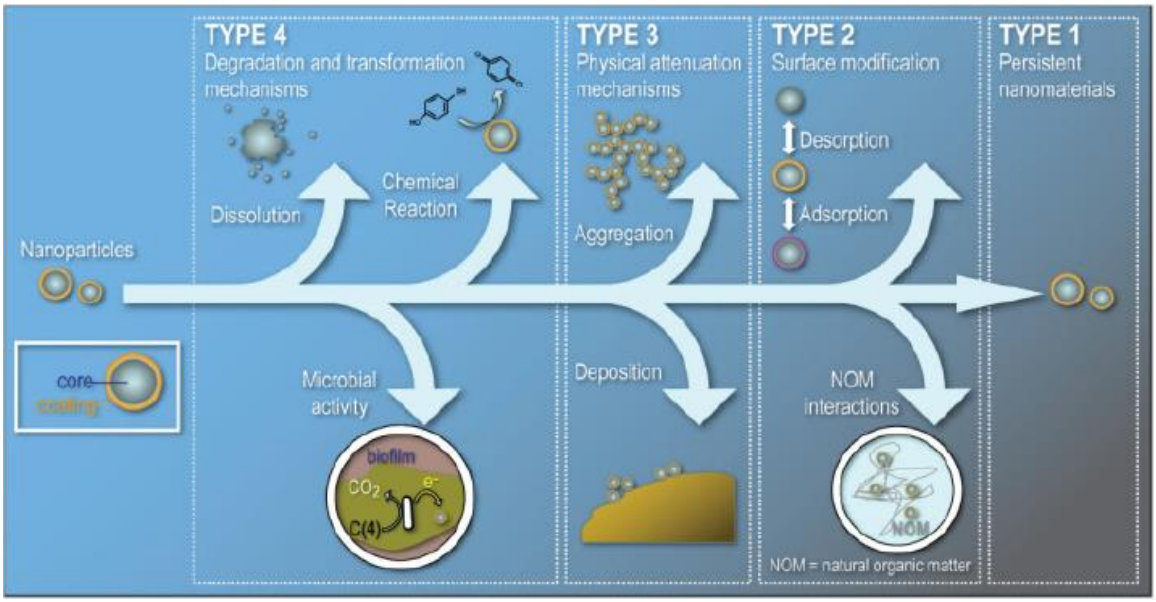

Figure 2.9 Nanoparticle Transformation and Environmental Fate. [54]

This particle transformation can affect any combination of physicochemical properties. Changes to size, surface chemistry, and other properties then lead to a change in environmental fate and biological effect. The result of this transformation in properties and effects means that studying the toxicity of "pristine" or as-synthesized nanoparticles is insufficient to determine the full impact of specific ENMs. [29]

II.5 Exposure and Risk from Chemical Mechanical Planarization

The development and use of engineered nanomaterials over the past two decades have raised concerns regarding the risk of working with or near the manufacturing process as well as environmental effects. [14, 41, 42, 44, 57] By 2020, the number of workers in nanotechnology related industries is expected to be 6 million with a third of that in the United States. [56] In particular, high throughput users of nanomaterials in the

electronics industry for chemical mechanical planarization (CMP) are of epidemiological interest. CMP uses metal oxide nanoparticles at high concentrations in a slurry which can become aerosolized and expose workers in nanofabrication facilities. Existing literature on the subject is limited, with a few case studies on those that work in CMP fabs, with others looking at the hazards of process effluent or the nanoparticles themselves [8, 31, 35, 37,41, 42, 44, 46, 50, 51, 52, 53]

A study conducted by Dr. Sara Brenner at the SUNY College of Nanoscale Sciences looked directly at the incidental nanoparticles present in a CMP fab and those near the wastewater treatment facility. Filter-based sample collectors were worn by workers to mimic inhalation routes of exposure while also utilizing direct-read particle counters to determine the relative quantity and size of airborne particles. This study found that there were an increased number of nanoparticles in the air around specific CMP related tasks. These results suggested that CMP nanoparticles can become aerosolized and potentially be hazardous to workers. [4,5]

CHAPTER III

PHYSICOCHEMICAL CHARACTERIZATION OF NANOPARTICLE SLURRIES BEFORE AND AFTER COMMON CMP PROCESSES

III.1 Introduction

Chemical Mechanical Planarization (CMP) is a polishing technique used in the semiconductor industry to thin and flatten stacked layers of metal and dielectric materials in the manufacture of integrated circuits and similar devices. As the name suggest, removal of material occurs through both chemical and mechanical methods with the ratio varying process-to-process. CMP slurries are formulated to provide an abrasive in the form of nanoparticles suspended in ultrapure water with any number of chemical additives at a specific pH to promote the desired removal mechanism. For example, popular CMP processes for the removal of copper utilize a Silica nanoparticle in a basic pH solution with a triazole compound additive. In this scenario, the SiO2 nanoparticle can be sized according to amount of abrasion desired, while the high pH chemically etches and the triazole inhibits copper corrosion post-process.

An illustration of the major CMP components is shown in figure 3.1. An inverted wafer is held by the carrier and pressed into a polish pad with precise forces exerted downward. The pad and carrier rotate, and the polish arm moves back and forth across the radius of the pad. While this is happening, slurry is constantly flowed across the pad

to perform the polishing. For some processes such as SiO_2 polishing, an abrasive conditioner continuously rejuvenates the pad surface at the same time. [21, 38]

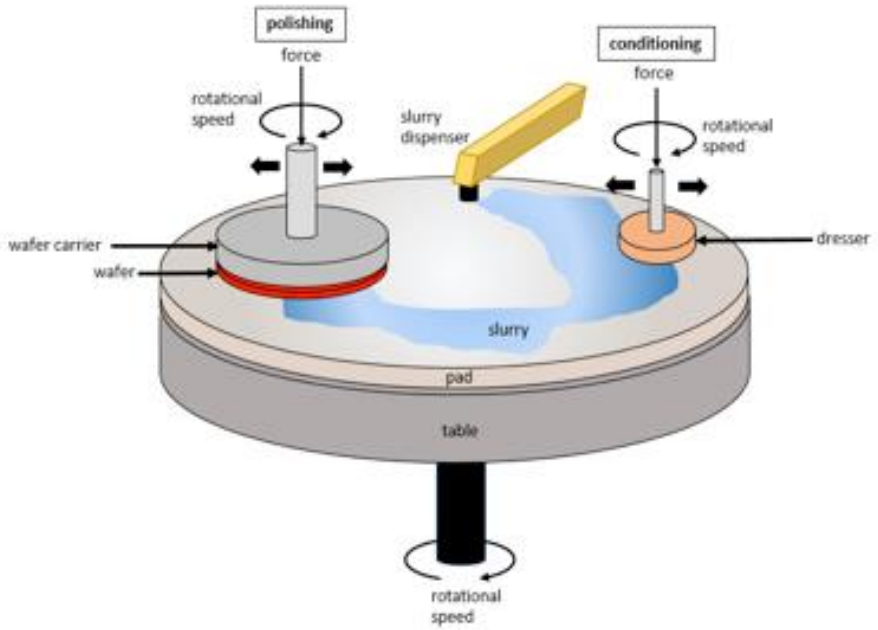

Figure 3.1 Depiction of CMP Components. [30]

Some processes use no additives beyond the nanoparticles whereas other processes utilize additives to slow drying, chelate removed material, or simply color the slurry. Regardless of composition, slurries used for CMP interact with the polished substrate at a chemical and mechanical level which can modify not just the polished surface but the slurry itself. Apart from the addition of the removed material, the nanoparticles may roughen or smooth, develop surface chemistries, and change in size. In the interest of environmental health and safety, it is important to understand not just the composition of CMP slurry as it is purchased, but also the form in which it goes down the drain. [8, 18, 31, 38, 43, 47]

The first step in assessing the toxicity of the nanoparticles in CMP waste begins with physicochemical characterization of the slurry before and after polishing to determine if any transformation occurred. The slurries that contain transformed nanoparticles may also vary in biological interactions and a varied physicochemical characteristic may correlate with that biological change. Since everything in the waste must be known and controlled the extent it can, it is important to have as much control and knowledge of the CMP process itself. To that end, the CMP processing done to generate the waste for this study was done specifically for this study; simple SEMI-standard wafers were polished using popular off-the-shelf industrial CMP slurries on a production-grade CMP tool but in an isolated university cleanroom area with dedicated drain for the collection of waste.

III.2 Methods

III.2.1 Chemical Mechanical Planarization and waste collection

A wide variety of CMP processes are currently used in semiconductor cleanroom globally. For this study, some of the most common slurry/substrate combinations were used. To capture the breadth of materials used, processes that used both benign and hazardous materials for the nanoparticle slurry and substrate were selected. SiO_2 is generally considered safe in many forms and is both the most common nanoparticle material and removed material as a dielectric film in devices. Using SiO_2 NPs to polish SiO_2 films was therefore considered a benign process due to benign/benign components. However, even SiO_2 NPs can be made in a variety of ways, some of which can be more toxic. Using a similar SiO_2 slurry to polish highly toxic III/V materials such as GaAs

(detailed in chapter V) is considered a benign/hazardous process. Metal oxide slurries such as Al_2O_3 and CeO_2 were selected as having higher toxic potential compared to SiO_2 NPs based on current literature. To explore the transformation and toxic potential of a variety of processes, the following CMP combinations were processed and collected:

Table 3.1 CMP Processes Used.

Slurry/Nanoparticle Composition	Slurry name	Intended Use	Substrate Materials Polished
30nm colloidal SiO_2, 9.5 pH	Eminess Ultra-sol® 200s	III/V and optics	SiO_2, GaAs
50nm colloidal SiO_2, 10.4 pH, triazole additive	DOW ACuPLANE™ LK393C4	Cu barrier	Cu
140nm fumed SiO_2, 10.9 pH	Cabot Semi-sperse® 12E	Interlayer dielectric (ILD), shallow trench isolation (STI)	SiO_2
170nm CeO_2,	AGCEM CES 333F-2.5	ILD, STI	SiO_2
240nm Al_2O_3, 4.1 pH	Eminess Ultra-sol® A20	Metal removal	Cu

Process parameters for each configuration were selected based on process quality. To generate waste that would be realistic but also most likely to exhibit some nanoparticle transformation, high removal rates with acceptable polish results were used. These values are included in Appendix 1. All polishes were done on a Speedfam-IPEC Avanti 472 using a DOW IC1000 polish pad on a single platen (no final polish) with new pads for each process and a full tool cleaning to prevent cross-contamination. Slurries were drained directly into precleaned collection bottles via inert PFA tubing.

III.2.2 Size and surface charge

Collected CMP waste and pristine slurry samples were thoroughly agitated and pipetted into sample tubes for analysis preparation. All samples were diluted 1000x in ultrapure DI water and vortexed for 1 minute. Using a syringe, 1mL of the dilute slurry solution was immediately injected into disposable folded capillary cells for DLS/Zeta analysis in a Malvern Zetasizer Nano ZS. 10 readings were performed at room temperature per set.

Samples that had been diluted 1000x were diluted again 10-fold for a 10,000x total dilution from stock concentrations and mixed again. 200 mesh Cu TEM grids were made hydrophilic by 30s, 50w DC argon plasma. 2 microliters of each slurry and waste sample were pipetted onto the TEM grids and left covered in a clean container overnight to dry. Particle sizing was done by manual measurement in Olympus iTEM software using images obtained from a Zeiss Libra TEM using 120kv 5-8µA beam.

III.2.3 Chemical analysis

Pristine slurry and waste samples were pipetted at full concentration on a Pike MIRacle ATR stage in a Varian 670 FTIR and scanned for 64 samples to detect functional groups. Ultrapure DI water was used as a common background and pristine/waste samples were directly compared.

Pristine and waste samples were mixed and 5mL of each was digested for ICP analysis. SiO_2 containing samples were left in 1% HF for 24 hours, Al_2O_3 samples were left in Aluminum Etch Type A solution for 24 hours. Filtered samples were prepared by 5k MWCO Vivaspin 15 centrifuge tubes spun at 2500 xg for 60min. After mixing and

determining there was no sedimentation in sample tubes, samples were analyzed in a Varian 710-ES ICP-OES for elements in both the nanoparticles and substrates to determine dilution factor of waste and the concentration of removed materials. Additional ICP preparation and analysis was done for the GaAs polishing slurry as detailed in Chapter V.

III.3 Results and Discussion

III.3.1 Size and surface charge

Changes in the nanoparticles' size and surface charge was quantified by dynamic light scattering (DLS) techniques and examined by TEM for morphological changes. The nanoparticles in each slurry waste sample increased in hydrodynamic diameter from the original pristine slurry, with the larger colloidal silica increasing the least with +7.3% or less than 7nm on average. The largest change was in the smaller 30nm colloidal silica after the SiO_2 polish, though this +94.4% size increase was also accompanied by a larger size spread of nearly 35nm. Values for each slurry type are listed below in table 3.2.

Changes in zeta potential, or surface charge, closely reflected the changes seen in size. The specific changes in waste samples' absolute value increased or decreased by as much as 22% from their original values in the pristine slurry. While the GaAs polished nanoparticles increased in value and became more soluble, the fumed silica used to polish SiO_2 decreased, or became less soluble, by a similar amount. The other processes had more marginal differences of around 10% or less. Full values for each are listed below in table 3.3.

The slight size increase and surface charge modification following CMP processing is logical based on what is happening to the slurry during a standard polish. Chemical interactions between the slurry additives, nanoparticles, and polished substrate occur while the nanoparticles are simultaneously being pressed into and moved along the surface that is being polished. Whether through primarily chemical or mechanical means, the slurry becomes a solution of substrate material in ionic or particulate form due to this slurry interaction. The nanoparticles themselves can become an aggregation or adsorption site for the removed material. Additionally, direct chemical interaction during the polish process can cause nanoparticles to have modified surface groups or charges as well. Ultimately, the result is what was measured in the DLS results; an increase in size and modified surface charge due to this buildup of removed material or direct modification by the CMP process.

To further assess any related size or morphology changes, nanoparticles from each slurry sample were imaged by transmission electron microscopy (TEM). Unlike with DLS, measurements made by TEM must be done manually, particle-by-particle. The nanoparticles are also dried and prepared for vacuum compared to the solution-based DLS measurement. By TEM, there was no discernable difference between pristine slurry samples and waste except for the GaAs polish, which is further explored in the following chapter. This apparent conflict with the DLS results can be attributed to the different sample preparation methods. Loose substrate material that is aggregating around the nanoparticles or bound to its surface by intermolecular forces may not be visible in a dried sample.

If the nanoparticles were physically ground by the CMP process in such a way that the particle size *reduced* considerably, this would be visible by TEM. Similarly, if nanoparticles became significantly smoother or rougher due to the process, this could also be observed. While it is not expected that either of these cases occurred in the processes done as a part of this study, there is also the possibility that only certain nanoparticles are directly affected by the CMP process. All the slurries selected for this study, and most of those available commercially, range from 1-30% total dissolved solids in the form of nanoparticles. The sheer number of nanoparticles, coupled with the manner in which slurry is continuously sprayed onto the CMP polish pad, means that only a fraction of the total CMP nanoparticles actually make contact with the polished surface. This amount will vary greatly by the specific process conditions and tool efficiency, but it is possible and even likely that the majority of the nanoparticles in waste samples did not take direct involvement in substrate removal. The hypothesized nanoparticle transformation is more likely for nanoparticles in direct contact with the removal process, so even if transformation takes place, it will be with a smaller fraction of the total particles present. Methods like DLS allow for the analysis and quantification of large numbers of nanoparticles at once, allowing even a minority of nanoparticles with different characteristics to skew the average. These uncommon transformed nanoparticles may be more difficult to assess by direct imaging techniques, so the lack of discernable difference by TEM is not unusual. Representative TEM images for each slurry are shown below.

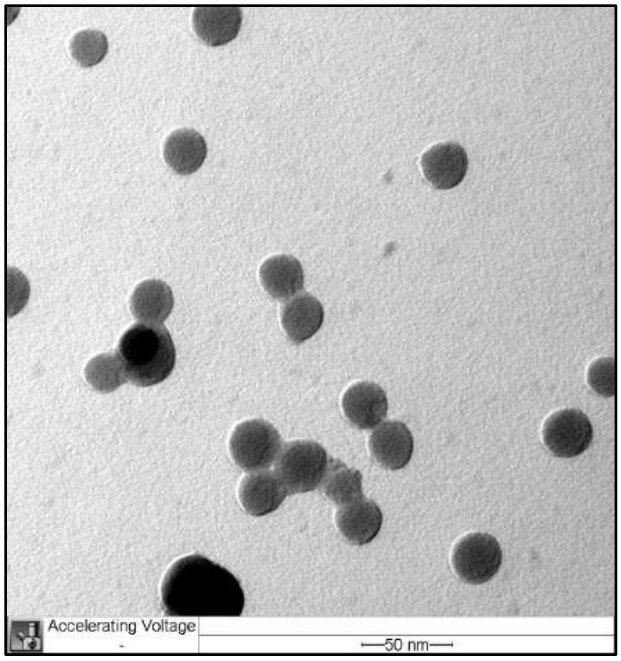

Figure 3.2 30nm Colloidal Silica Slurry, 63000x TEM Image.

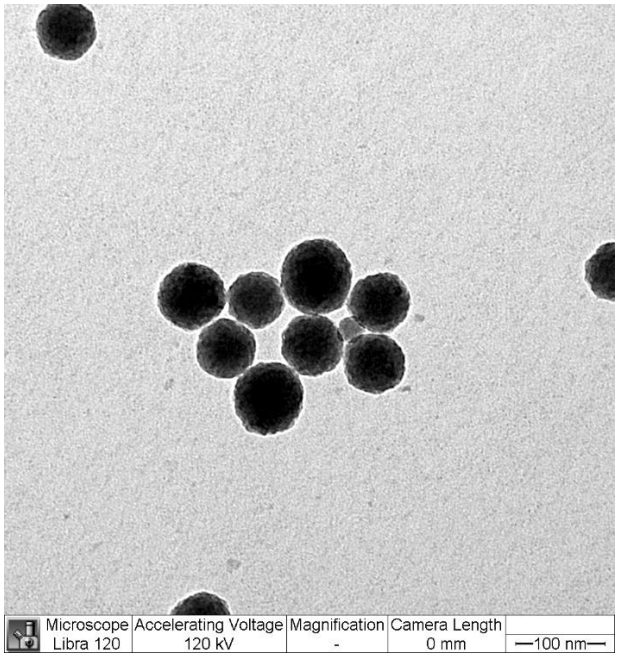

Figure 3.3 50nm Colloidal Silica Slurry, 50000x TEM Image.

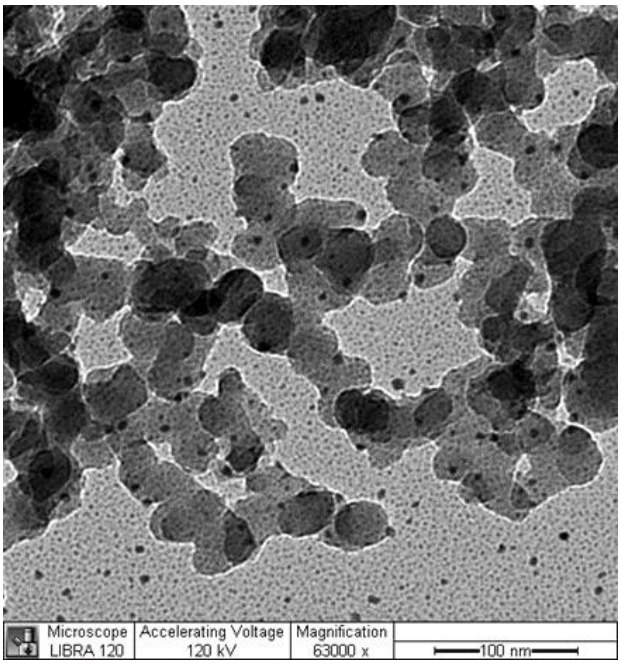

Figure 3.4 140nm Fumed Silica Slurry, 63000x TEM Image.

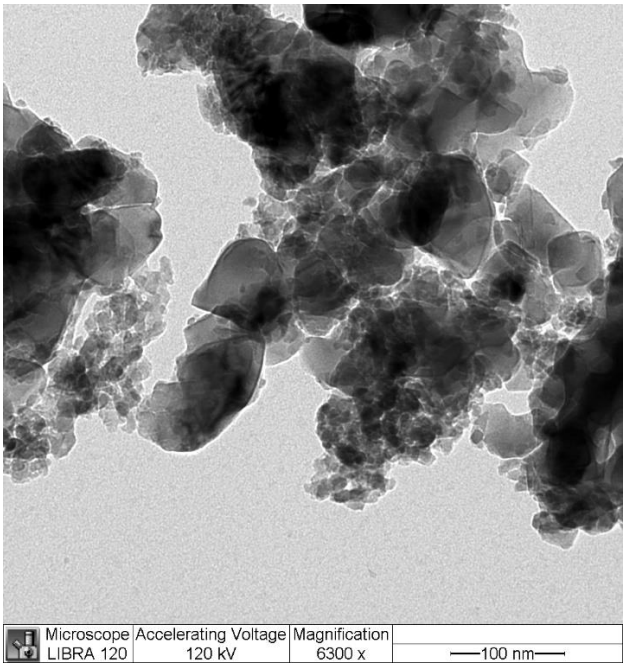

Figure 3.5 240nm Alumina Slurry, 63000x TEM Image.

Table 3.2 Slurry and Waste Size Distribution from DLS.

	Pristine Slurry		Waste		
Slurry (Process)	Value (nm)	Standard Deviation	Value (nm)	Standard Deviation	% Change
30nm SiO_2 (SiO_2)	31.18	8.89	60.62	34.93	+94.4%
30nm SiO_2 (GaAs)	-	-	35.14	10.57	+41%
90nm SiO_2 (Cu)	90.49	19.99	97.16	26.26	+7.3%
140nm f-SiO_2 (SiO_2)	152.2	68.3	166.5	77	+9.4%
170nm CeO_2 (SiO_2)	203.6	87.9	225.3	131.4	+10.7%
240nm Al_2O_3 (Cu)	578.7	291.3	927.3	321.8	+60.2%

Table 3.3 Slurry and Waste Zeta Potential Distribution from DLS.

	Pristine Slurry		Waste		
Slurry (Process)	Value (nm)	Standard Deviation	Value (nm)	Standard Deviation	% Change
30nm SiO_2 (SiO_2)	-34.9	16.0	-31.0	10.5	-11.2%
30nm SiO_2 (GaAs)	-	-	-42.2	12.8	+20.9%
50nm SiO_2 (Cu)	-42.2	11.5	-40.5	13.2	-4.0%
140nm f-SiO_2 (SiO_2)	-48.8	8.3	-38	7.15	-22.1%
170nm CeO_2 (SiO_2)	-42.3	8.26	-43.4	18.1	+2.6%
240nm Al_2O_3 (Cu)	11.1	3.74	10.2	6.1	+8.1%

III.3.2 Chemical analysis

Similarly, this capacity for minor change in a subset of nanoparticles may be the reason no real chemical difference was detectable as well. Wet slurry samples analyzed by FTIR as well as dried samples analyzed by X-ray photoelectron spectroscopy did not exhibit any changes in the pre-versus post-polish slurries (data not shown). It is hypothesized that any chemical transformation, such as that which caused the difference in DLS size and zeta potential, is minor and affects only a subset of particles. In other words, the changes are below the detectable limits of these techniques. The other possibility that no such transformation took place, though due to the chemical nature of the CMP process, further study should be done to better determine the presence or absence of any chemical shift on the particles' surfaces. If the nanoparticles directly affected by the process could be isolated from or concentrated, any changes may be detectable. More sensitive instrumentation or techniques may also be able to detect any differences.

ICP analysis was done to detect copper content in the silica and alumina waste slurries used in that process. To determine if the Cu present was present as free ions, the waste was filtered using 3,000 kDa centrifuge filters and the Cu content compared. The results are shown in figure 3.6. The 90nm SiO_2 waste had 67.9% of its copper content removed by filtration and 48.8% from the 240nm alumina waste. This suggests the filtered copper was either associating with the nanoparticles which were also trapped or forming particles large enough to be caught individually (>1-3nm).

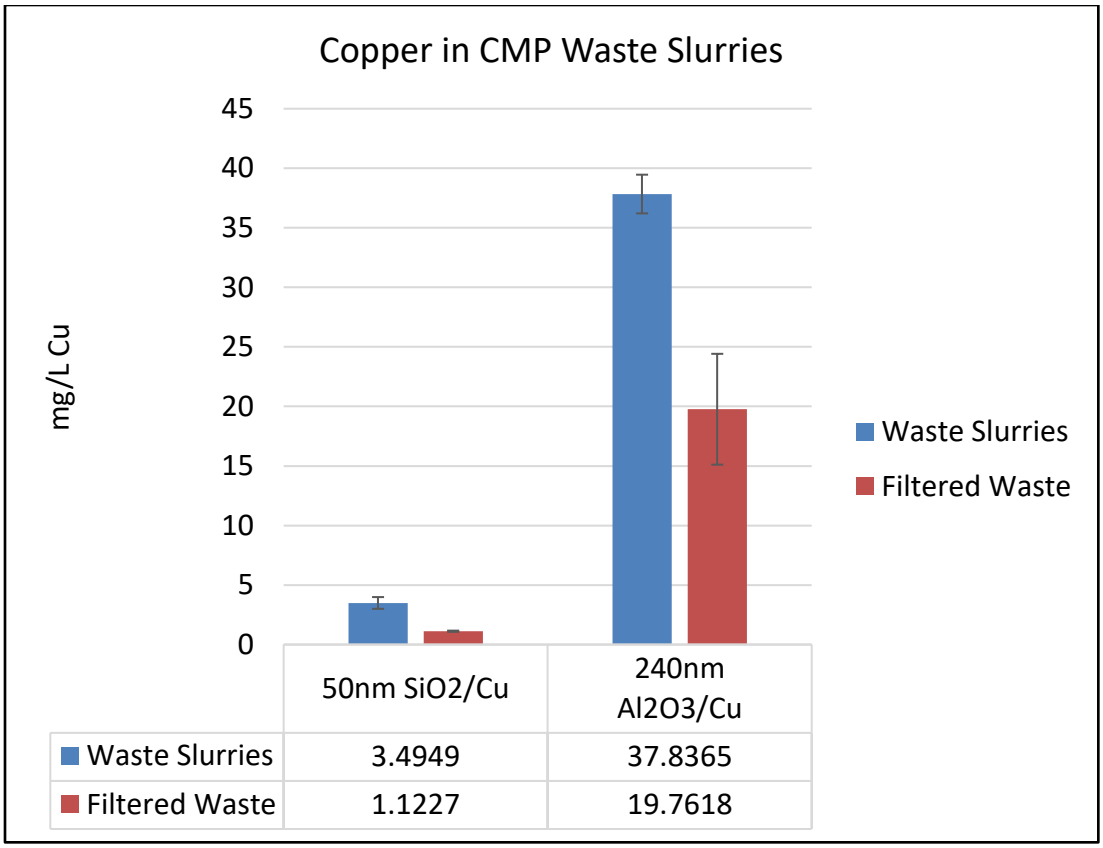

Figure 3.6 Copper Content and Filter Retention in Waste Slurries.

III.4 Conclusions

To study the possibility for nanoparticle transformation due to CMP processing, several different common processes were selected. Different types of silica, alumina, and ceria slurries were used to polish SiO_2, copper, and GaAs. The resulting waste was compared to new off-the-shelf slurry to determine what transformation took place. For these slurry and process combinations, minor changes were detected for all samples. DLS showed an increase in hydrodynamic diameter and a shift in surface charge for all waste samples.

TEM and various other chemical analysis did not show an apparent difference between waste and pristine slurry samples, potentially due to having a small subset of the nanoparticles interact with the substrate and transform. Transformed characteristics may also be below the detection limit. Additional study is needed to further elucidate the extent and nature of the transformation from these processes. If the ratio of transformed (or affected) nanoparticles can be increased, this would enable detection and study. Only the GaAs polish process showed additional transformation, which is discussed in Chapter V.

The first aim of this study, to demonstrate nanoparticle transformation due to CMP processing, was somewhat successful. While the changes were minor, an increase in size can affect biological interactions and toxicity. While a variety of processes were explored in this study, future work may focus on pushing one process to an extreme, or reusing slurry, as a worst-case-scenario for nanoparticle interaction and transformation due to the CMP process. Additionally, as there are numerous other processes and

parameters, different combinations may also yield different results and transformation potential. For the sake of this research, the waste generated was sufficient to move to the next step, assessing toxicity and biological interactions.

CHAPTER IV

CYTOTOXICITY OF NANOPARTICLE SLURRIES BEFORE AND AFTER COMMON CMP PROCESSES

IV.1 Introduction

Nanoparticle toxicity is dependent on physical as well as chemical properties. Among many different types of NPs, size, shape, and surface chemistry-dependency has been reported in literature as discussed in Chapter II. The nanoparticles from CMP waste will have their own biological effects as well; these effects may change slightly in their behavior or toxicity levels due to the physicochemical transformation discussed in Chapter III. The contents of this chapter follow the objectives from the specific aims 2 and 3 that guided this research. Common general cell assays and cell uptake were tested across the broad variety of CMP processes and conditions discussed previously using three different cell lines. The cell lines were selected based on common routes of exposure, representing the lungs, liver, and immune system. [28]

IV.2 Methods

IV.2.1 Cell selection and culture methods

Due to the exposure routes of interest (inhalation, ingestion), three cell lines were selected for study. A549 lung epithelial cells, HepG2 liver epithelial cells, and RAW 264.7 macrophages. Lung epithelial cells are the first to encounter foreign contaminants

when inhaled. If ingested, nanoparticles come to the liver (hepatic first pass effect). Macrophages are in the bloodstream and serve as part of the immune system and phagocytose particles. [75] All cells are established immortalized cell lines for continuous cell culture and only low-passage cells (<20) were used for this study. Toxicity assays were done in sterile 96w polystyrene cell culture treated plates with conditions in triplicate wells. Cells were seeded at 2,000 cells/well and allowed to grow for 24h before dosing or beginning the assay.

IV.2.2 Cell assays

Cell viability, or metabolic activity, was measured using a resazurin dye. Alamar Blue was purchased from Thermo Fisher Scientific, a resazurin-based indicator for overall cell metabolic activity. Resazurin is cell permeable and becomes reduced by the healthy cellular environment into resofurin, detectable with a distinct color change and increase in fluorescence. After the 24h growth period, cells were dosed with various concentrations of silica, alumina, or ceria slurry samples and left to grow in an incubator at 37 C and 5% CO2 for 48h. At the end of 48 hours, the 100µL in each well was supplemented with 10µL Alamar Blue reagent for 2 hours in the incubator. At the end of this period, the cells were read on a fluorescence plate reader, excitation wavelength 545 and emission wavelength 590. Results are expressed as a percent of negative control (undosed cells).

Cell necrosis was determined by LDH release, using the LDH release assay from Sigma Aldrich. In this test, cell media is aspirated off from adherent cell cultures after the dosing period and lactate dehydrogenase (LDH), a cytosolic enzyme present in most

cell types, is present in greater amounts if the cells have ruptured cell membranes. This extracellular LDH is measured by an enzymatic reaction where it catalyzes lactate to pyruvate by NAD+ reduction to NADH. This NADH then reduces a tetrazolium salt to a detectable red formazan product. Cells were dosed and grown for 48h in the same manner as the Alamar blue assay. At the end of the incubation period, 50µL supernatant from each well was transferred to a different plate. 100µL of the LDH kit reagent mix was added and the plate was incubated at room temperature for 30min. Absorbance was measured on a plate reader at 490nm. These values were reduced by 690nm background levels.

Oxidative stress was measured using a general ROS H2DCFDA reagent from Thermo Fisher Scientific. In this assay, the cell permeable reagent (2',7'-dichlorodihydrofluorescein diacetate or H_2DCFDA) has acetate groups cleaved by intracellular esterases and oxidation, converting it into the fluorescent DCF product (2',7'-dichlorofluorescein). After the 24h growth period, cells were exposed to the DCFDA reagent then dosed for 4h. After 4h in the incubator at 37 C and 5% CO2, plates were read on the plate reader with excitation 492nm, emission 522nm.

The apoptosis assay was purchased as a Caspase 3/7 Green kit from Thermo Fisher Scientific for plate reader use. CellEvent Caspase 3/7 uses a four amino acid peptide (DEVD) that has been conjugated to a nucleic acid binding dye. Once in the cell, the conjugation site can be cleaved by activated caspase-3/7 in apoptotic cells, allowing the dye to bind to nearby nucleic acids and emit fluorescence. After the 24h growth period, cells were dosed with the reagent at 6µM and the slurry samples for 4h. After

that time, results were read on the plate reader using settings for excitation 488nm, emission 530nm.

IV.2.3 Cell uptake

Total nanoparticle uptake was also analyzed for each slurry sample and cell type. This was assessed using a quantitative and qualitative means to examine any potential changes due to transformation from a numerical or visual perspective. A Varian 710-ES Inductively coupled plasma-optical emission spectroscopy (ICP-OES) instrument was used to quantify nanoparticle uptake, whereas a Cytoviva darkfield microscope was used to directly image cells using established method. [27] All slurry samples and cell line combinations were analyzed as with the previous assays.

To quantify uptake, cells were cultured in a similar manner to the assays above prior to analysis by ICP-OES. 6-well microplates were used to increase total cell count and 24-hour dosing time were used at relatively low concentrations to minimize cell death. After culturing, the cell media was removed, the plates washed gently with PBS, and cells were digested directly in the plates. These nanoparticle-containing cell pellets were digested using acids relevant to the nanoparticle composition. Silica-containing cells were digested in 10% hydrofluoric acid, while ceria- and alumina-containing cells were digested with a 50/50 ratio of aluminum etchant type A and 5% nitric acid. The aluminum etchant type A composition was 80% phosphoric acid, 5% acetic acid, 5% nitric acid, and 10% deionized water. All digests were given 72 hours on a plate shaker rotating at 300rpm before solutions were mixed and collected for ICP analysis. [12]

For microscope imaging nanoparticles in cells, a slightly different culture method was used. Cell cultures were seeded in BD Falcon™ chambered cell culture slides and allowed to grow for 48 hours, reaching approximately 50% confluency. The chambers were then dosed at 50 mg/L for 12 hours, well below any toxicity threshold for these nanoparticles. After dosing, media was removed and replaced with 4% formaldehyde in PBS for 15min at room temperature, then washed 3 times for 5min with PBS solution. Once the chambers were removed from the slide, Fisher Chemical™ Permount™ mounting media was applied and coverslipped using 50x24mm 1.0mm thick Thermo Scientific™ Gold Seal™ cover slips. Prepared slides were then imaged using a Cytoviva® dual oil-immersion darkfield microscope with QImaging® QI695 color CCD camera with Ocular™ acquisition software.

IV.3 Results and Discussion

IV.3.1 Cell selection and culture methods

The purpose of this set of experiments was primarily to assess any discernable differences in biological effect between an off-the-shelf pristine CMP slurry and the used form that makes up CMP waste effluent. Although several different nanoparticle types were used (alumina, ceria, silica), this study was not intended to compare the various chemistries. Due to the various sizes and slurry compositions used, direct cross-comparisons are not meaningful. Ideally, those nanoparticles that were most transformed in aim 1, described in the previous chapter, would be most closely evaluated for a shift in biological effect. Due to the fact that there was a modest shift in size and zeta potential for most particles but no drastic or chemical transformation, all slurries were evaluated

for any potential biological changes that may have been due to this small shift in physical characteristics or some unseen transformation.

The cells used represent those commonly affected by nanoparticle exposure; A549 human alveolar basal epithelial cells represent the lining of the lungs for inhalation. Hep G2 human liver epithelial cells are relevant to nanoparticles that are ingested and absorbed along with nutrients. The RAW 264.7 cells are mouse macrophage cells and results from their use indicate the interaction of immune blood cells with nanoparticles that enter the bloodstream. While some cells have varying sensitivity to nanoparticle induced toxicity, the goal of this study was again to expose any potential differences caused by nanoparticle transformation. Secondary to this goal, the data regarding the relative toxicity of each cell type to a given nanoparticle type is informative.

IV.3.2 Cell assays

Using a wide range of dosing concentrations, a level of effective toxicity was detected for all nanoparticles and cell types. Some materials were only mildly toxic and a full dose curve for viability could not be fully shown due to a high-end limit to what is feasible or relevant. Stock slurries at lower concentrations (<10%) were dosed up to 2 g/L, higher concentration (10-30%) were dosed up to 10 g/L. Such a high concentration would also require separate culturing and assay methodology due to the media displacement and opacity of the resulting solution. To summarize the 33 sample combinations, IC_{50} values, or the concentration at which a cell line was only at 50% the viability of its negative control, is listed in Table 4.1. Those with values in excess of the relevant concentration range are marked accordingly.

Cellular viability showed some toxicity to all nanoparticle types, general trends from literature were reflected in the results. Generally speaking, larger alumina and ceria nanoparticles were not as toxic as the smaller silica nanoparticles. The 30nm colloidal silica particles were more toxic than the 90nm colloidal silica particles, while the 140nm fumed silica nanoparticles were significantly more toxic than the 90nm colloidal silica and similar to the 30nm colloidal silica (.5 g/L fumed versus 0.3 g/L colloidal), despite being much larger. As discussed in the literature review, this relatively higher toxicity in the fumed silica is likely due to its increased surface area or roughness compared to the perfectly round colloidal silica nanoparticles. This roughness may cause the nanoparticles to stick more readily to cell membranes, rupturing them and causing toxicity. Representative dose curves for the 30nm colloidal silica and 140nm fumed silica are shown in figure 4.1.

In the LDH release assay, the same trends are seen. Lower IC_{50} results from the viability assay showed generally higher membrane damage at similar concentrations. The largest ceria and alumina nanoparticles showed little to no membrane damage in this assay. In A549 lung epithelial cells, 30nm colloidal silica and 140nm fumed silica nanoparticle slurries both showed greater than twice the leaked LDH of the negative control at less than 1g/L. However, the fumed silica showed greater total membrane damage at 1 and 2 g/L above 4x the negative control while the colloidal silica was well below 3x at those concentrations, as shown in figure 4.2.

As mentioned previously, the intent of this study was not to compare relative toxicity levels of different nanoparticle types or even cell types. While the general trends

in the data match what is known from literature, the ultimate goal was to assess the difference between the toxicity of pristine, new slurry and the CMP waste that has been transformed by the polishing process. In this pursuit, it is notable that there was no discernable difference in pre- versus post-polish nanoparticle toxicity for any combination of the nanoparticles and cell types. This applies to both the general viability and membrane damage assays. On one hand, it has been clearly demonstrated in the greater body of nanotoxicity literature and reinforced here that there are size-dependent toxicity trends among nanoparticles of similar composition. The muted physical transformation does not yield a discernable difference. A larger difference in particle size would cause a change in toxicity, though the precise amount of change for each particle required is unknown. The membrane damage and viability did not show any difference in the waste nanoparticles compared to the new slurry, but apoptosis and ROS generation rates did have an effect.

Several of the waste slurries did not significantly increase or decrease the amount of ROS generated in the cells, as show in figure 4.4. The alumina nanoparticles used to polish copper films did have a significant increase in ROS for all three cell lines. This increase is most likely due to the higher copper content discussed in Chapter III. The silica used to polish copper did not have the same increase but had much lower copper quantities due to a lower removal rate during CMP. Conversely, ROS production was decreased in ceria waste samples that were used to polish SiO_2. Ceria nanoparticles have been shown in literature to prevent oxidative stress by serving as oxygen stores, easily switching between valence states. It is likely in the case of this waste slurry that

the functionalized or modified surface of the nanoparticles is modified in chemical state to allow this mechanism to take place. No detectable difference was present, but a small unnoticed change could have allowed the antioxidant effect to take place.

Apoptosis rates were also changed in waste slurry samples compared to the new nanoparticles. Nearly all cell and nanoparticle combinations yielded a significant difference as shown in figure 4.3. Interestingly, there is no clear pattern as rates go up or down for different condition sets. As with the previous results, the changes are likely due to small imperceptible surface modifications and the aggregation of substrate material around the nanoparticle. It is possible that the nanoparticles are bringing this extra material into contact with the cell and causing it to disrupt cellular processes in different ways. This result requires exploration in future work. There are 2 main apoptosis pathways and a number of biomolecules that could be probed to determine what precisely is being affected by each nanoparticle combination.

Table 4.1 Cell Viability After 48-Hour Nanoparticle Dose, IC_{50} Values.

Slurry nanoparticle composition/process	A549 lung epithelial	HepG2 liver epithelial	RAW 264.7 Macrophage
30nm SiO_2 New	0.30 g/L	0.20 g/L	0.19 g/L
30nm $SiO2/SiO_2$	0.32 g/L	.23 g/L	0.18 g/L
30nm SiO2/GaAs	0.28 g/L	0.20 g/L	0.12 g/L
90nm SiO_2 New	*>10 g/L*	*>2 g/L*	0.5 g/L
90nm SiO_2/Cu	6.5 g/L	*>2 g/L*	0.8 g/L
140nm f-SiO_2 New	0.54 g/L	0.22 g/L	0.28 g/L
140nm f-SiO_2/SiO_2	0.62 g/L	0.25 g/L	0.38 g/L
200nm CeO_2 New	*>2 g/L*	*>2 g/L*	*>2 g/L*
200nm CeO_2/SiO_2	*>2 g/L*	*>2 g/L*	*>2 g/L*
240nm Al_2O_3 New	*>10 g/L*	4.2 g/L	5.8 g/L
240nm Al_2O_3/Cu	6.6 g/L	3.5 g/L	6.5 g/L

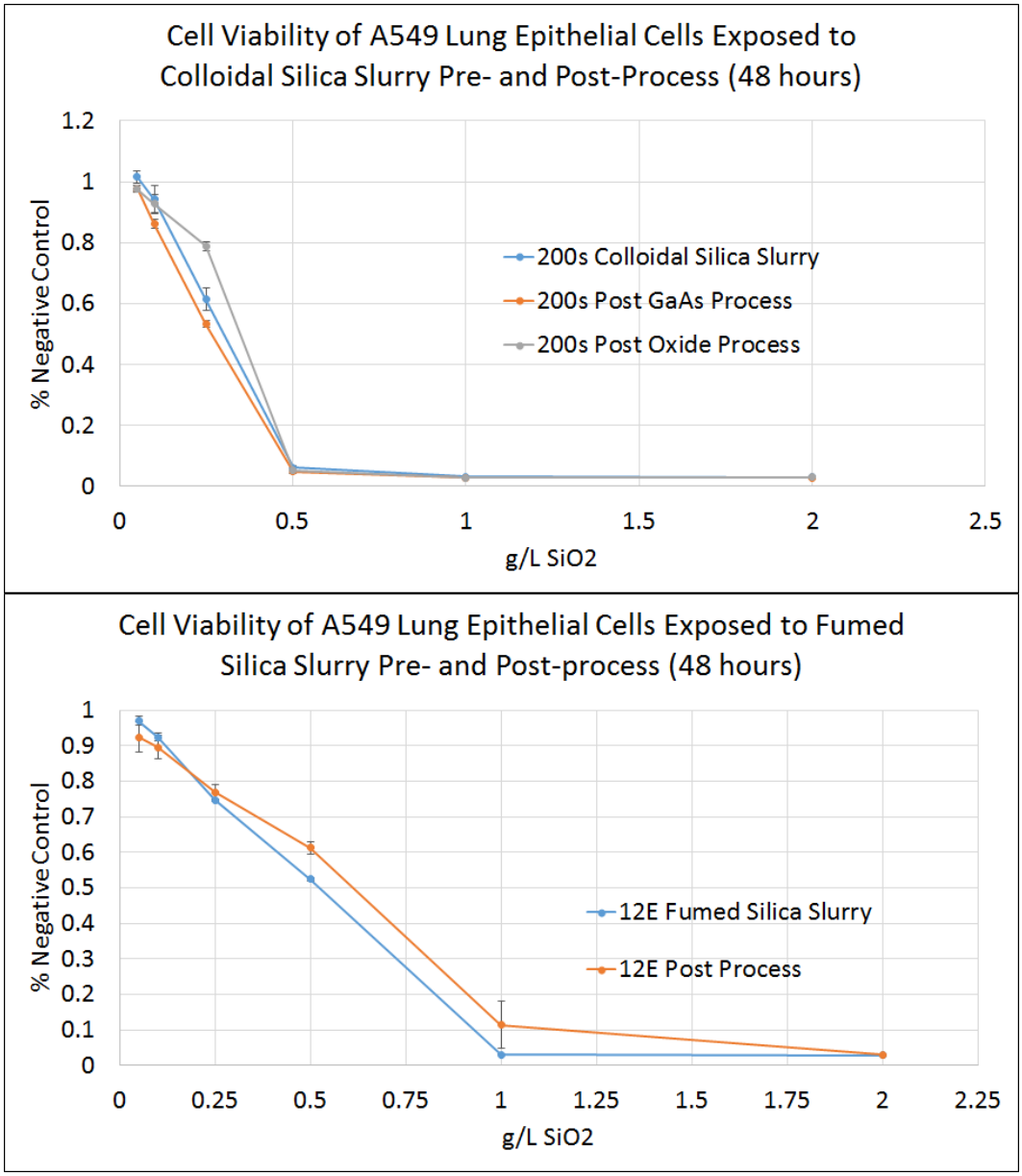

Figure 4.1 Cell Viability of A549 Lung Epithelial Cells Exposed to 30nm Colloidal Silica (top) and 140nm Fumed Silica (bottom).

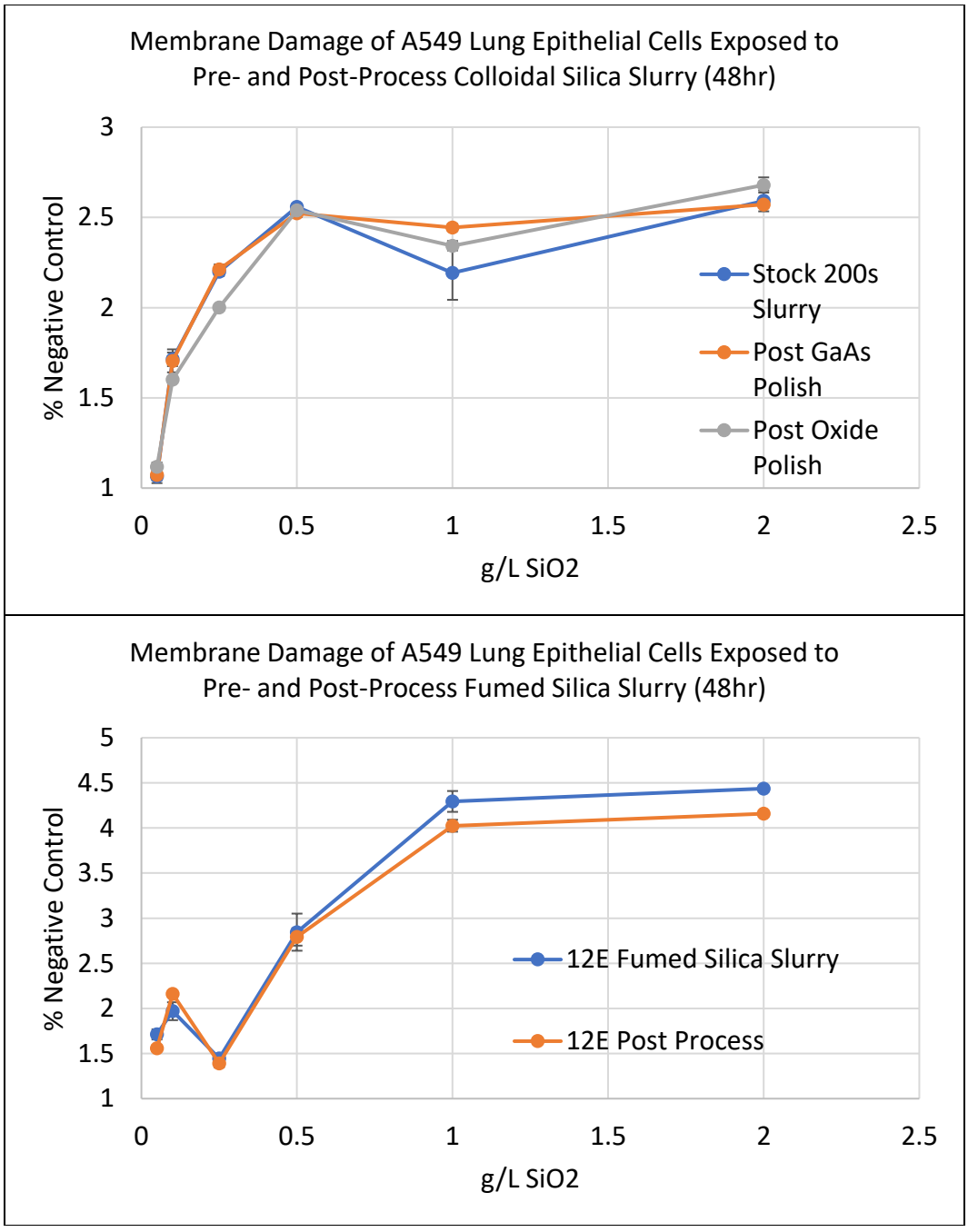

Figure 4.2 Membrane Damage of A549 Lung Epithelial Cells Exposed to 30nm Colloidal Silica (top) and 140nm Fumed Silica (bottom).

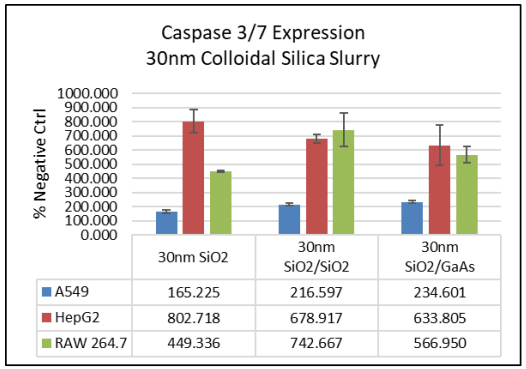

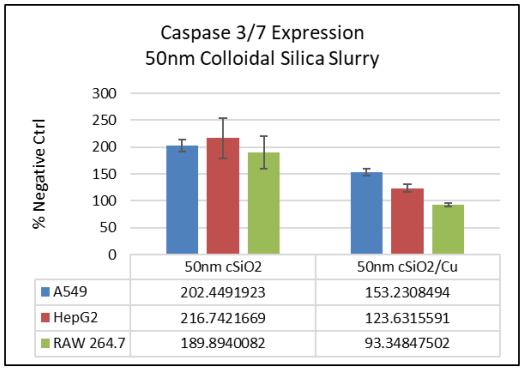

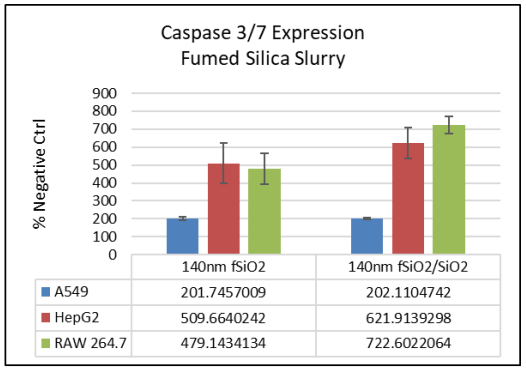

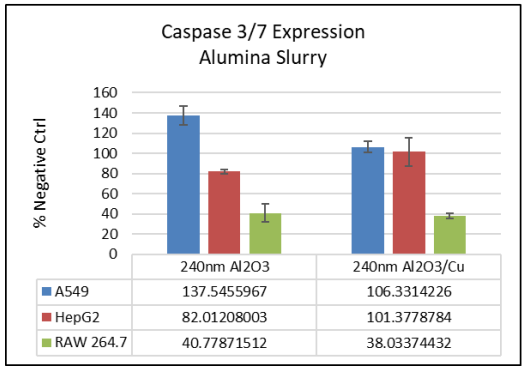

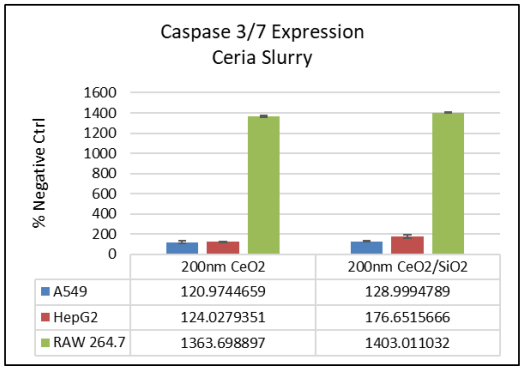

Student's T-test, p-values			
	A549	HEPG2	RAW 264.7
30nm SiO2	*	*	*
30nm SiO2/SiO2	**0.0019**	**0.0330**	**0.0093**
30nm SiO2/GaAs	**0.0029**	**0.0210**	**0.0202**
50nm SiO2	*	*	*
50nm SiO2/Cu	**0.0002**	**0.0028**	**0.0246**
140nm fSiO2	*	*	*
140nm fSiO2/SiO2	*0.9476*	**0.0322**	**0.0024**
200nm CeO2	*	*	*
200nm CeO2/SiO2	*0.0568*	**0.0350**	**0.0131**
240nm Al2O3	*	*	*
240nm Al2O3/Cu	**0.0010**	**0.0007**	*0.5751*

Figure 4.3 Apoptosis Assay Results.

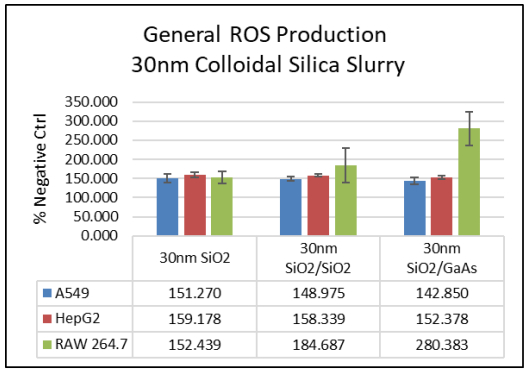

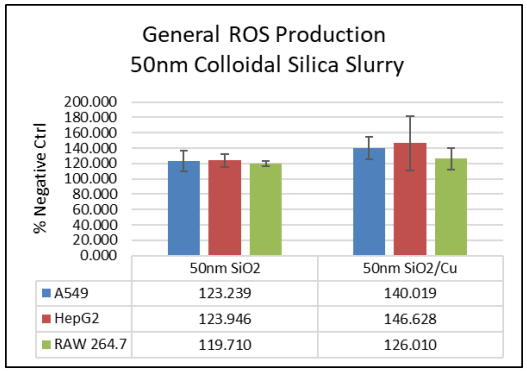

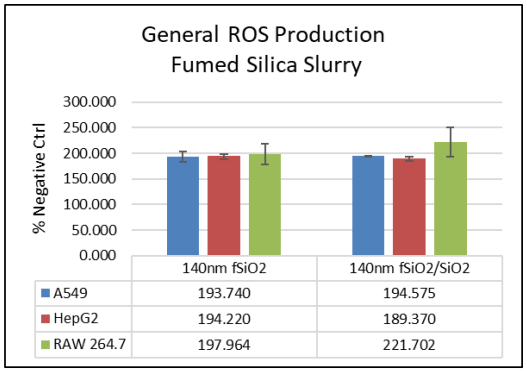

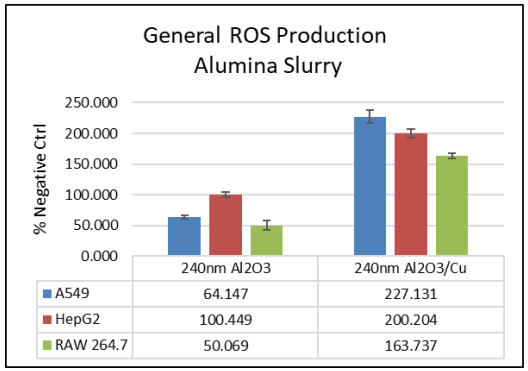

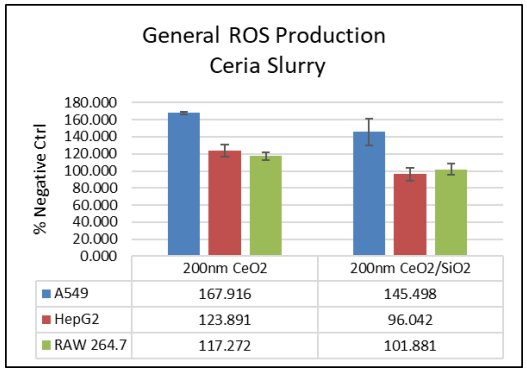

Student's T-test, p-values			
	A549	HEPG2	RAW 264.7
30nm SiO2	*	*	*
30nm SiO2/SiO2	*0.71870*	*0.83545*	*0.23325*
30nm SiO2/GaAs	*0.27695*	*0.12444*	**0.00147**
50nm SiO2	*	*	*
50nm SiO2/Cu	*0.21463*	*0.34142*	*0.50527*
140nm fSiO2	*	*	*
140nm fSiO2/SiO2	*0.88132*	*0.18437*	*0.22426*
200nm CeO2	*	*	*
200nm CeO2/SiO2	*0.07358*	**0.00814**	**0.03012**
240nm Al2O3	*	*	*
240nm Al2O3/Cu	**0.00001**	**0.00001**	**0.00002**

Figure 4.4 Reactive Oxygen Species Assay Results.

IV.3.3 Cell uptake

Total cell uptake of nanoparticles is an important metric for the evaluation of overall toxicity. Toxicity in general is caused by the direct physical or chemical interaction of nanoparticles with cellular processes and biomolecules. Nanoparticles that can readily enter the cell are more likely to interact with these processes and create a toxic effect. The objective of this research was to compare the amount of new and waste nanoparticles taken up by cells to determine if there was any change in interaction that may stem from nanoparticle transformation. This was performed by ICP-OES analysis to determine the total amount of silica, ceria, or alumina in cell lysates as well as direct imaging using a darkfield microscope capable of imaging nanoparticles.

The results of ICP analysis are shown in table 4.2, 4.3, and 4.4, divided by cell lines. There are minor changes but no large increases or decreases. Similarly, microscope images such as figures 4.5 through 4.15 showed uptake but no change in the waste. Based on the data gathered from characterization and the assays detailed above, this is an expected result. A major shift in toxicity or transformation would have been more likely to yield a major change in uptake. The images show a large uptake in the smaller nanoparticles whereas the largest alumina has very few nanoparticles per cell. This is supported by the ICP data which showed less alumina than any other nanoparticle in all three cell lines. [49]

Table 4.2 Nanoparticle Uptake in RAW 264.7 Macrophages Determined by ICP-OES.

RAW 264.7 Macrophage Cells	**Pristine Slurry**	**Waste**
Slurry (Process)	Value (mg/L)	Value (mg/L)
30nm SiO_2 (SiO_2)	6.94±0.46	6.07±0.87
30nm SiO_2 (GaAs)	-	7.912±0.35
50nm SiO_2 (Cu)	4.62±0.35	3.95±0.37
140nm f-SiO_2 (SiO_2)	6.46±0.07	7.60±0.39
170nm CeO_2 (SiO_2)	10.86±0.18	16.40±0.50
240nm Al_2O_3 (Cu)	1.08±0.07	1.06±0.08

Table 4.3 Nanoparticle Uptake in A549 Lung Epithelial Cells by ICP-OES.

A549 Lung Epithelial Cells	**Pristine Slurry**	**Waste**
Slurry (Process)	Value (mg/L)	Value (mg/L)
30nm SiO_2 (SiO_2)	7.05±0.28	6.87±0.34
30nm SiO_2 (GaAs)	-	8.44±0.55
50nm SiO_2 (Cu)	3.81±0.03	4.29±0.20
140nm f-SiO_2 (SiO_2)	5.01±0.15	7.52±0.07
170nm CeO_2 (SiO_2)	4.75±0.16	3.96±0.10
240nm Al_2O_3 (Cu)	1.28±0.10	1.04±0.20

Table 4.4 Nanoparticle Uptake in Hep-G2 Liver Epithelial Cells by ICP-OES.

Hep-G2 Liver Epithelial Cells	**Pristine Slurry**	**Waste**
Slurry (Process)	Value (mg/L)	Value (mg/L)
30nm SiO_2 (SiO_2)	4.18±0.16	3.77±0.34
30nm SiO_2 (GaAs)	-	4.23±0.16
50nm SiO_2 (Cu)	3.96±0.46	4.40±0.36
140nm f-SiO_2 (SiO_2)	4.34±0.26	7.27±0.14
170nm CeO_2 (SiO_2)	8.20±0.39	8.45±0.06
240nm Al_2O_3 (Cu)	1.20±0.19	1.20±0.11

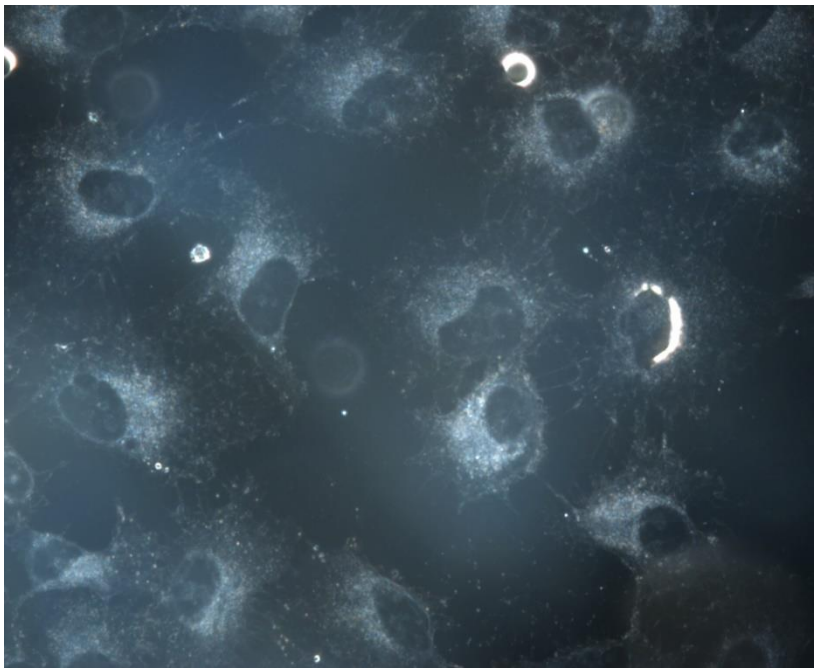

Figure 4.5 A549 Lung Epithelial Cells, 600x Magnification.

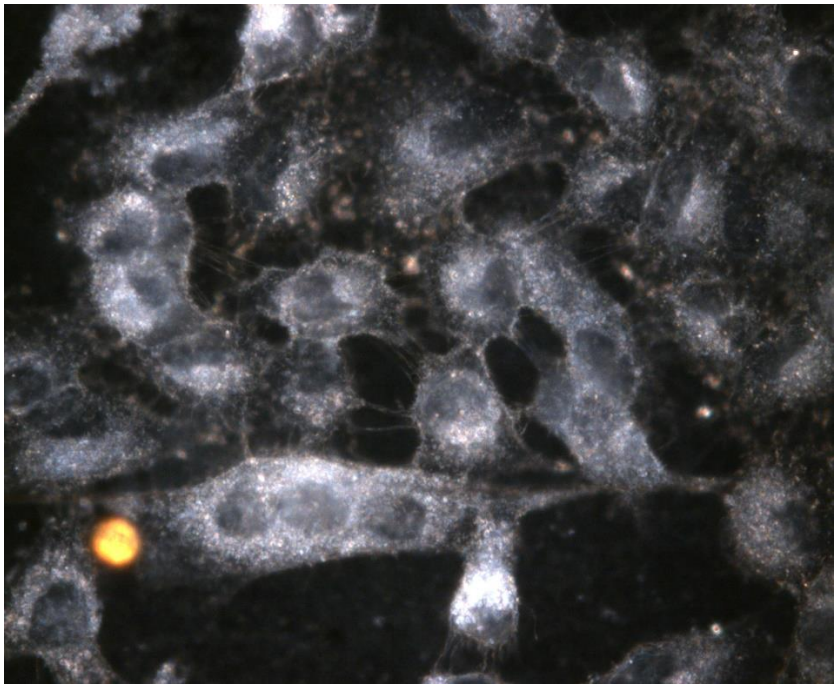

Figure 4.6 A549 Lung Epithelial Cells Exposed to 30nm SiO_2, 600x Magnification.

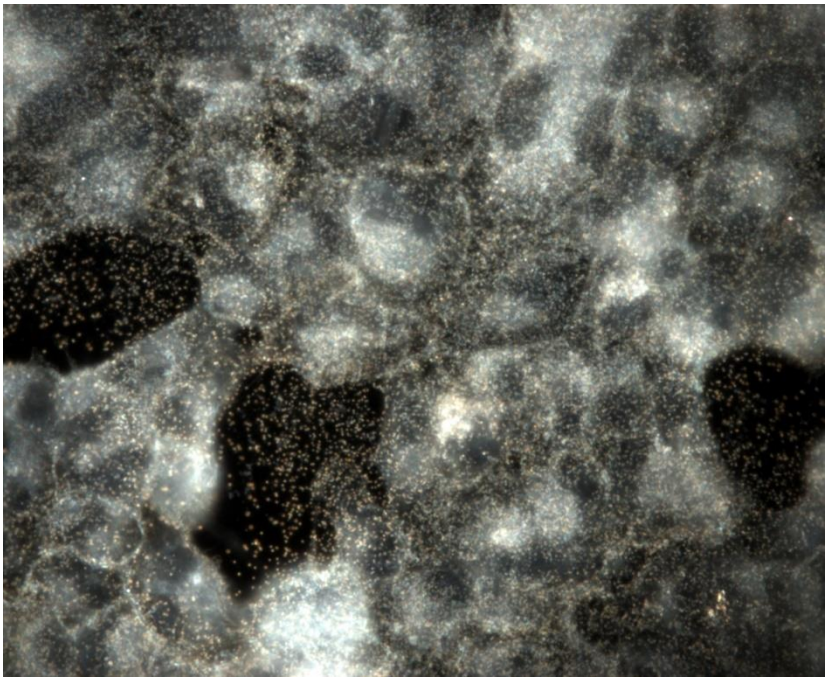

Figure 4.7 A549 Lung Epithelial Cells Exposed to 30nm SiO_2, 600x Magnification.

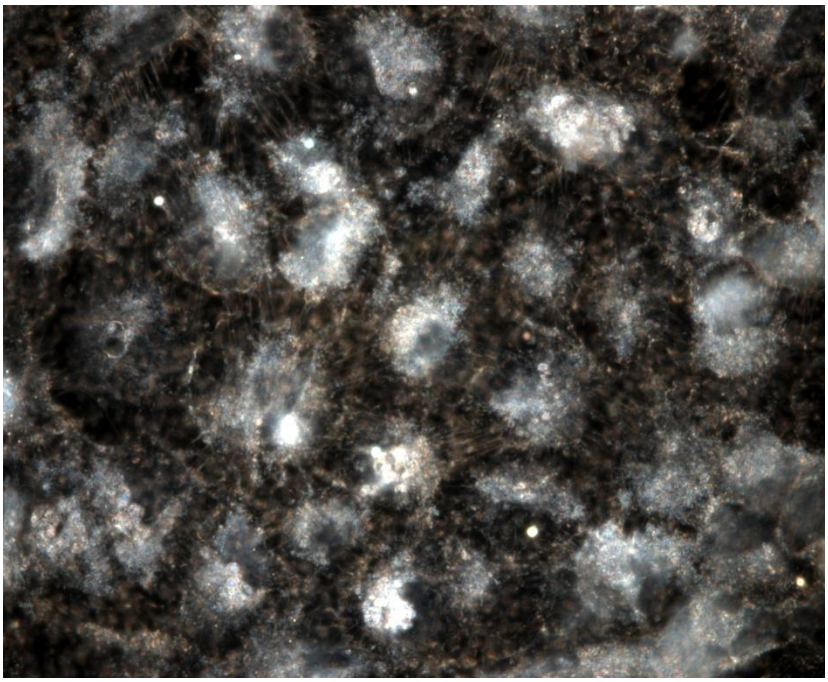

Figure 4.8 A549 Lung Epithelial Cells Exposed to 140nm fumed SiO_2, 600x Magnification.

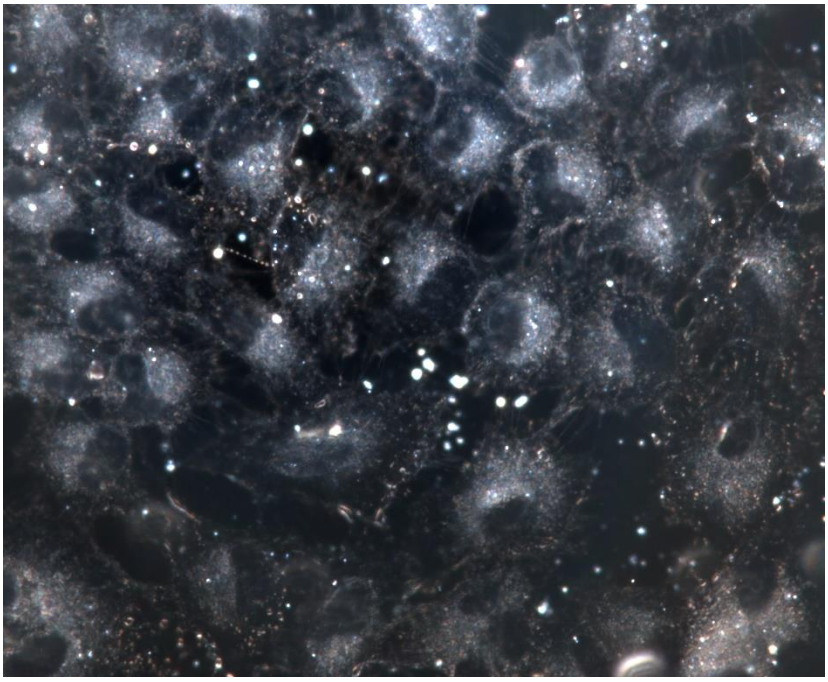

Figure 4.9 A549 Lung Epithelial Cells Exposed to 200nm CeO_2, 600x Magnification.

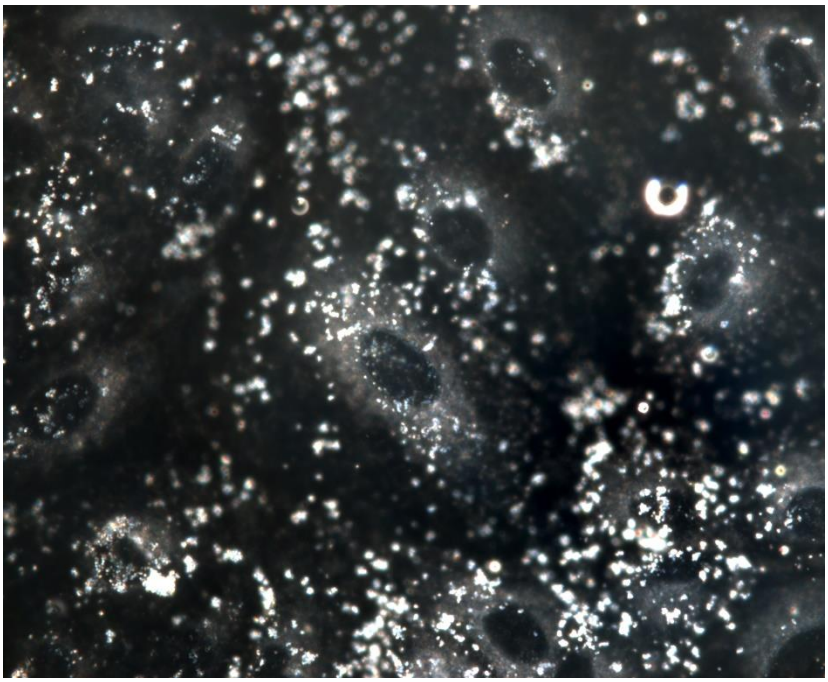

Figure 4.10 A549 Lung Epithelial Cells Exposed to 240nm Al_2O_3, 600x Magnification.

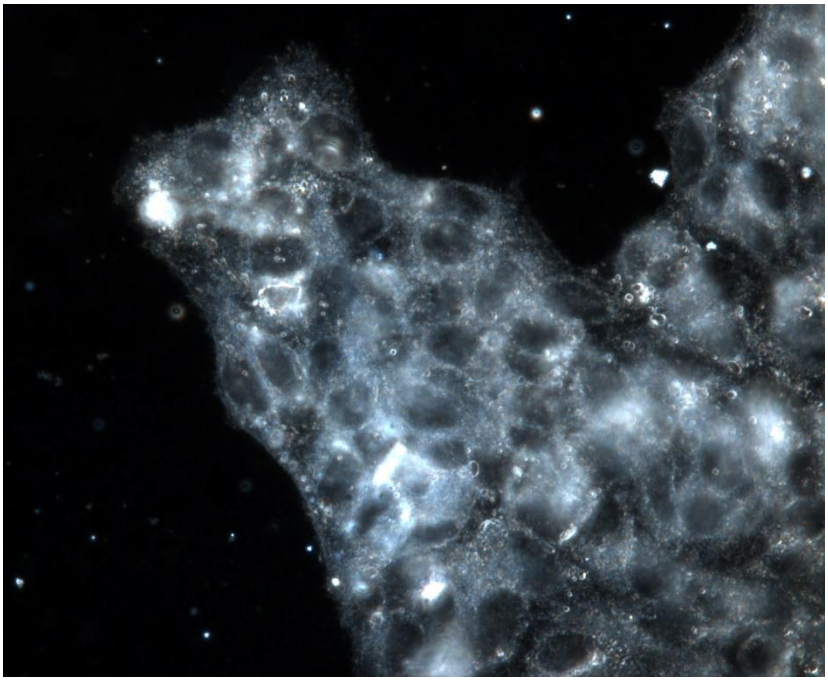

Figure 4.11 HepG2 Liver Epithelial Cells, 600x Magnification.

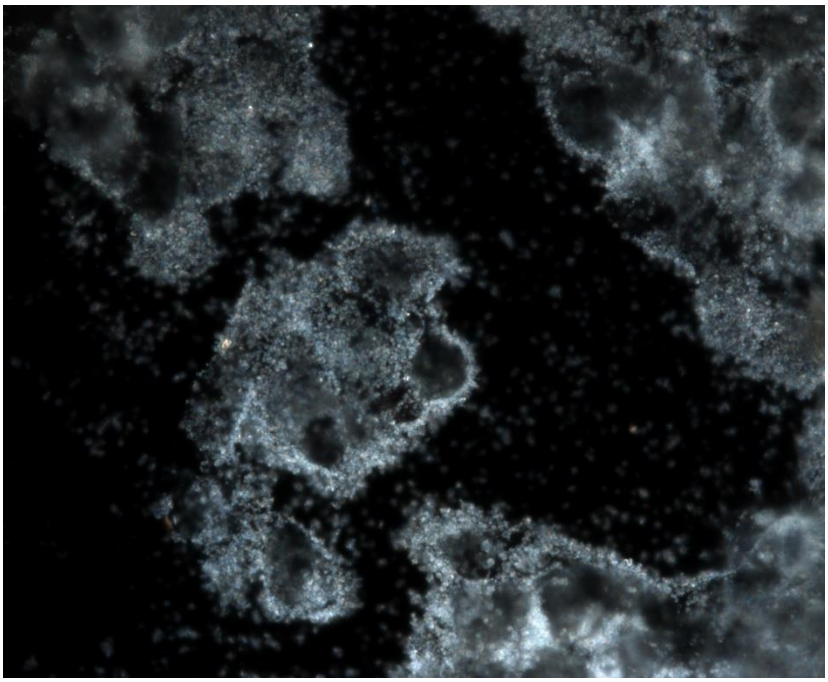

Figure 4.12 HepG2 Liver Epithelial Cells Exposed to 240nm Al_2O_3, 600x Magnification.

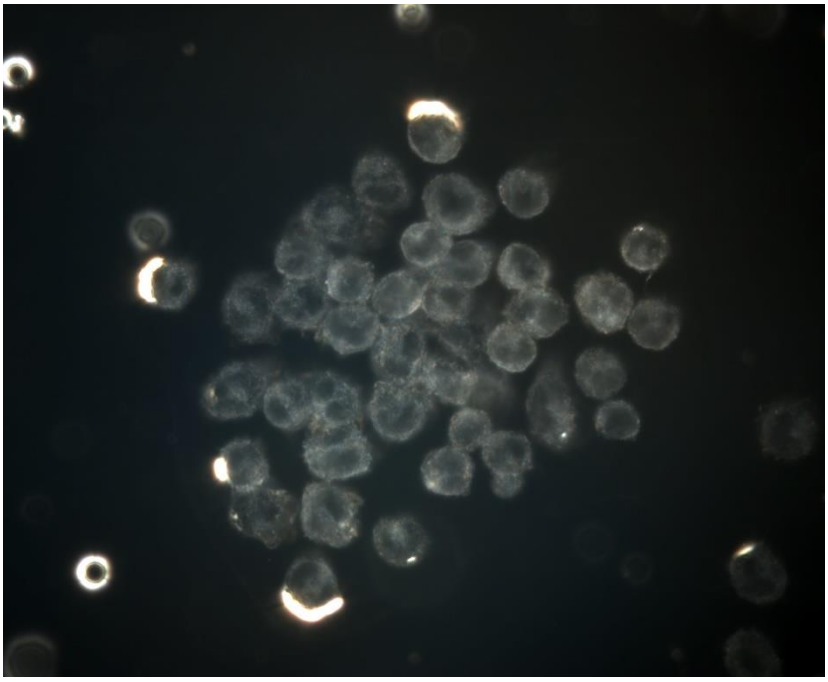

Figure 4.13 RAW 264.7 Macrophage Cells, 600x Magnification.

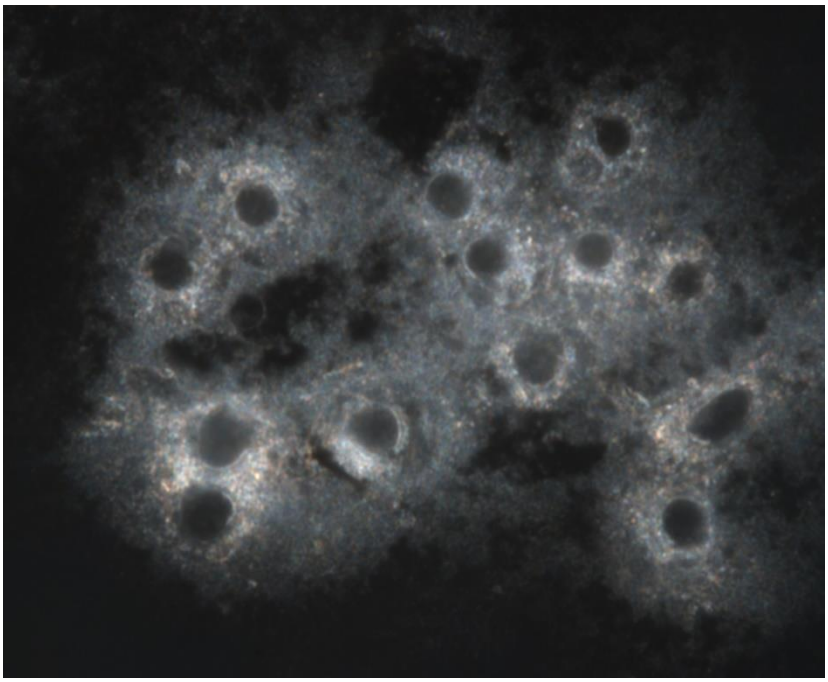

Figure 4.14 RAW 264.7 Macrophage Cells Exposed to 30nm SiO_2, 600x Magnification.

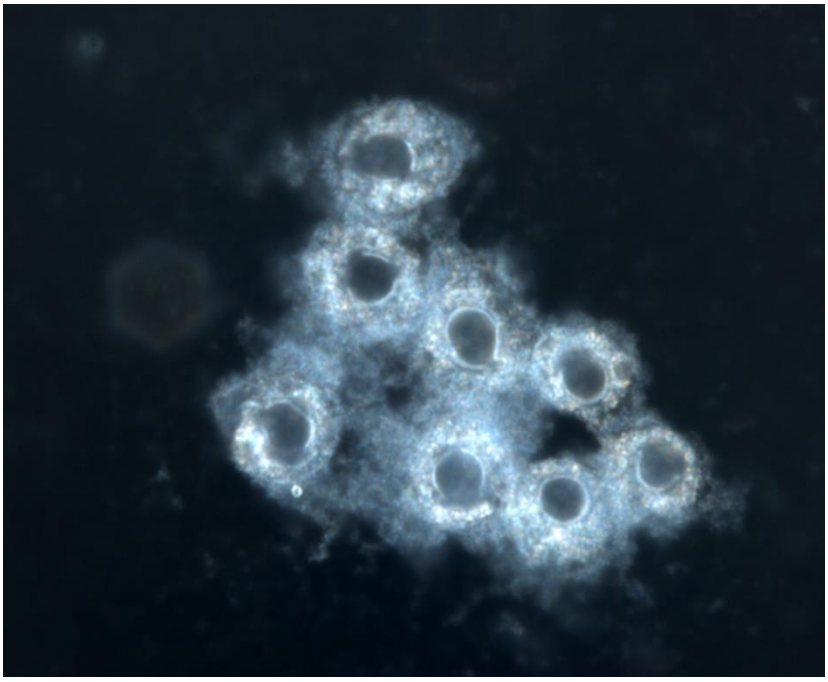

Figure 4.15 RAW 264.7 Macrophage Cells Exposed to 140nm fumed SiO_2, 600x Magnification.

IV.4 Conclusions

Among all the slurry and cell types, all nanoparticle samples caused a toxic effect in each cell type. Viability loss was minimal for the largest ceria and alumina particles, but dose curves were created for each slurry and cell type. While these toxicity thresholds were observed, there was minimal difference between the pristine slurry samples and waste samples. Similarly, necrosis was induced in a dose-dependent manner for all slurry and cell types, also without pristine/waste differences. Apoptosis showed some minor difference for most sample combinations and oxidative stress was increased by copper process waste slurries.

It is likely that the relatively minor physicochemical property shift was not strong enough to introduce a significant loss of viability or increased necrosis beyond the pristine slurry for these processes. Small parts of the substrate material may be associating with the NPs in solution, but this does not seem to play a role in necrosis or viability. Alternatively, these additional trace bits of substrate do seem to be slightly boosting apoptosis through an unknown mechanism. The particular pathway should be explored further to narrow down a specific mechanism. ROS was boosted in the post-copper sample for the alumina slurry, due to the significantly higher Cu content compared to the stock slurry, also higher than the colloidal silica Cu polish. This result is expected based on those properties due to Cu catalyzing hydroxyl radicals from H_2O_2 which cause this stress. Other slurry samples do not seem to significantly increase the ROS except for the SiO_2/GaAs sample, likely due to the slight amount of As in solution, a known toxicant.

CHAPTER V

ENVIRONMENTAL IMPACT AND SPECIATION ANALYSIS OF CMP WASTE FOLLOWING GaAs POLISHING

V.1 Introduction

In a push for faster and higher mobility devices and in the pursuit of beyond Moore devices, the semiconductor industry looks to materials such as III-V compounds (e.g. GaAs, InP) to replace or supplement silicon devices. [39,40] These compound semiconductors are often made of known potent toxicants (such as GaAs), which may have the potential to make process byproducts and waste hazardous from both occupational exposure and environment point of view. One such manufacturing process of concern is Chemical Mechanical Planarization (CMP) of III-V materials. CMP uses engineered nanoparticle (NP) slurries as a polishing abrasive for chemical and mechanical removal of semiconductor device layers in a well-controlled manner. The NPs from the slurry already constitute an occupational and environmental safety and health (ESH) concern that are being explored for various materials. [31, 35, 41] The addition of toxicants such as In, Ga and As are likely to increase this potential hazard. [44] However, little is known about the environmental fate, behavior, and biological impact of these waste. [4] After performing CMP on III-V layers, potent toxicants such as Arsenic may combine with slurry NPs or become aerosolized (e.g. AsH3 gas), potentially worsening the occupational toxicity and EHS impact of CMP waste effluents. The

objectives of this work are to study the ESH impacts of GaAs CMP waste, specifically on the (a) presence and speciation of Arsenic in the wastewater effluent; (b) physicochemical properties of the slurry nanoparticles and removed material after polishing; and (c) effect of collected CMP wastes on human health, primarily cytotoxicity.

It is important to understand not only the physicochemical properties and toxicity of slurry NPs and III-V materials, but also that of the transformed NPs and resultant waste. As previously mentioned, CMP typically has two modes of action that may occur in varying magnitudes: (a) the chemical etching of a substrate by the chemical composition and pH of the slurry and (b) the mechanical action from the slurry nanoparticle abrasives as they press against the rotating substrate. In a predominantly chemical process, the slurry particles may not undergo much physical change and much of the removed material can expect to be in a dissolved or ionic state. More mechanical processes may only result in small difference in the chemical composition of the slurry while the slurry particles themselves may change size and shape, along with the removed material present as a second population of particles in the wastewater. Following GaAs removal, the material may ionize from the chemical etching of the substrate as the highly toxic As(III) or As(V) and/or may come off as Ga or As particles from the CMP's mechanical action. Depending on its composition, the resulting waste may require different modes of remediation or treatment as well as may have varying toxic effects. Knowing which As species are present in GaAs CMP waste is important for waste treatment and discharge point of view. By measuring As species from a variety of GaAs

CMP process conditions, we can discern the key factors affecting the balance of As(III) and As(V) in the CMP waste.

Using an industrial CMP tool to polish GaAs substrates, post-CMP waste were analyzed and compared to pristine CMP slurry in this study, along with assessing their toxicity. The physicochemical properties of both the slurry NPs and the removed GaAs from the substrate were analyzed, including the species of Arsenic present in CMP waste. The toxicity level of the slurry and mode of cell death were also assessed using A549 lung epithelial and HEPG2 liver epithelial cells. The results from this research may help determine the specific effects of CMP slurry and processing conditions on wastewater containing elevated levels of Arsenic as well as provide insight on the type and relevance of remediation methods.

V.2 Methods

V.2.1 Colloidal silica nanoparticle-based slurry and characterization of CMP slurries

Ultrasol 200s (Eminess Technologies, AZ) alkaline colloidal silica nanoparticle (NP) slurry was used to polish 150 mm GaAs wafers. NP concentration, size, and pH of the slurry were assessed. Particle size was measured using a Malvern Zetasizer Nano DLS system as well as on a Carl Zeiss Libra 120 Plus Transmission Electron Microscope (TEM). The zeta potential was evaluated using the Malvern Zetasizer Nano system. Silica NP, Ga, and As concentrations were determined with an Agilent 7500cx ICP-MS (Inductively Coupled Plasma-Mass Spectrometer)

V.2.2 Chemical Mechanical Planarization and etch of GaAs substrates

An IPEC Avanti 472 CMP tool was used to polish 150 mm GaAs wafers. An IC1000 K-groove polish pad was used with pad conditioning between each wafer. Slurry dilution and arm pressure were varied and all other conditions were held constant: platen speed (72 rpm), carrier speed (80 rpm), back pressure (2.0 psi), and 110s polish with 10s pre-wet step at 200 ml/min slurry flow rate. Slurry was dispensed either fully concentrated or diluted with deionized water 1:1. Concentrated slurry polishing was done at 3.5, 4.0, and 5.0 psi. Diluted slurry allowed for higher pressures to be used, namely 5.0 and 9.0 psi. Waste slurry was collected by plugging the tub basin drain and vacuum aspirating off the waste into clean HDPE collection containers. For comparison, GaAs coupons were also etched in baths of the same pristine CMP slurry for up to 72 hours at ambient conditions.

V.2.3 Aerosol sampling for incidental particles and arsine generation

A Honeywell Midas Detector with arsine sensor cartridge was run continuously during polishing with the sensor intake inside the CMP cabinet above the primary polish platen to detect any arsine gases (AsH3−xRx) generated. The detection limit of the arsine sensor was 25 ppb. The air above the platen was also monitored for the presence of any incidental particles that may be released during CMP. A mini particle sampler (MPS) apparatus (ECOMESURE, France) was used for continuous sampling during MP. A flow rate of 350 mL/min was used with Quantifoil 1.2/1.3 TEM grids with an effective capture range of 1nm-1µm. [8]

V.2.4 Post-process characterization and arsenic speciation

Arsenic speciation for DMA, MMA, As(III), and As(V) were done for all CMP waste and wet etched samples. The sample with the highest Arsenic level was also tested for As species, along with pH dependency (pH 3-11). Samples were filtered using EMD-Millipore Amicon Ultra-15 Centrifugal filter tubes (3 KDa, approximately 1nm pore) spun at 4000xg for 60 min. Species were separated in an Agilent 1260 Infinity Bioinert HPLC using ammonium phosphate buffer (pH 6.0, 10mM, 0.9 mL/min) flowing through a Hamilton PRX100 (5µm pore size, 4.1 x 150mm) that was connected directly to the ICP-MS sample inlet. Arsenic species were quantified using an Agilent 7500cx ICP-MS. Particle size, zeta potential, and Silica, Ga, As concentrations were also measured after the CMP process.

V.2.5 Cytotoxicity assays

A549 (ATCC CCl-185) lung epithelial and Hep G2 (ATCC HB-8065) liver epithelial cells were cultured in polystyrene plates using standard media formulations from ATCC and dosed with 0.1-2 g/L silica slurry for 48 hours. The pre- and post-CMP slurry samples were compared to As(III) and As(V) standards (SPEX CertiPrep). Cell viability was assessed using the Alamar blue assay (Thermo Fisher Scientific) to determine 50% inhibitory concentration (IC_{50}) for each sample. Membrane damage (indicative of necrosis) was also tested with the Lactate Dehydrogenase (LDH) release assay (Sigma-Aldrich). General reactive oxygen species was tested using the DCFDA assay (Abcam) and finally, cell apoptosis was tested with a Caspase 3/7 assay, Caspase-Glo (Promega). All assays were read on a Biotek Synergy 2 multi-mode plate reader.

V.3 Results and Discussion

V.3.1 Colloidal silica nanoparticle-based slurry and characterization of CMP slurries

Before CMP processing, the Ultrasol 200s slurry was characterized by the previously mentioned methods. The listed 30 nm NP size was measured to be 28.6±2.3nm by TEM and 31.18±8.89 by DLS. Figure 1 shows the morphology and size uniformity of the silica nanoparticles in the slurry. The zeta potential was -34.9±16, indicating moderate stability in water. CMP slurries frequently require continuous mixing while being used in the process, but Ultrasol 200s only requires occasional agitation, as per manufacturer recommendations. The silica content was measured (using ICP-MS of Si) was found to be 24.8±0.3%. Arsenic and gallium content in the pristine (stock) slurry was measured to be 32.04±1.24 µg/L and 0.05±0.01 µg/L respectively. Arsenic in the stock slurry is likely from impurities in the seed particle used to grow the colloidal silica NPs. The pH was measured to be 9.4, an appropriate alkalinity for the chemical etching of GaAs.

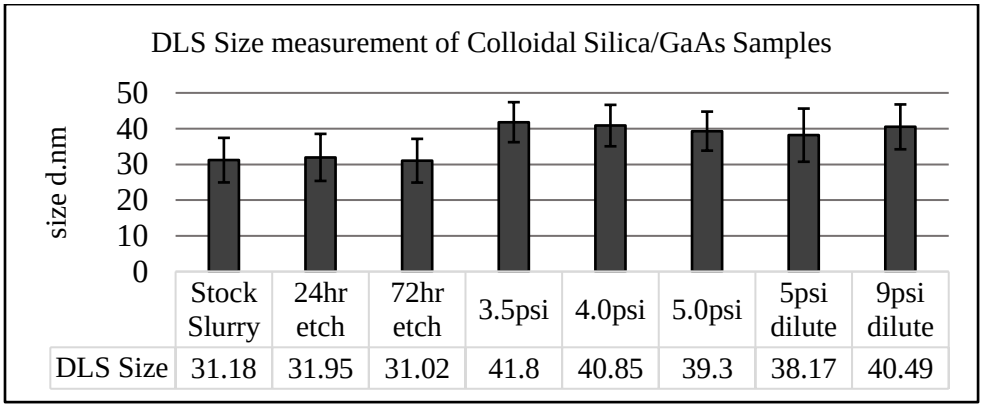

Figure 5.1 Size Distribution of Slurry NPs in Stock Slurry, Wet Etch Bath, and CMP Waste.

V.3.2 Chemical Mechanical Planarization and etch of GaAs substrates

Solid, SEMI standard 150 mm GaAs wafers were polished using a 50 mil IC1000 K-groove pad. While polishing, air sampling for incidental particles was done using an ECOMESURE MPS which has been shown to be effective in 5-150nm collection range (8). No particles were detected at any pressure condition, indicating that no particulate is aerosolized during the CMP process. Since CMP is an entirely wet process, this is not an unexpected result; dried particles will aerosolize readily. Arsine gas generation was also monitored using a toxic gas monitoring system sensor cartridge for AsHx gases. No arsine gas was detected, indicating that if any gas was generated, it would be below 25 ppb. Air was tested for arsine above the platen during the polish and for 15 min after CMP.

V.3.3 Post-process characterization

Slurry NPs used for CMP processing and wet etching were measured by DLS and compared to the stock NPs. The particles used in the GaAs etch showed no significant size change whereas particles from CMP waste showed a slight increase in size of 8-10 nm, as shown in Figure 5.1. This may indicate that the mechanical component of the CMP polish does have some transformative effect on the physical properties of the slurry NPs. Since the silica particles do not increase SiO_2 content from GaAs polishing, it seems likely that Ga and/or As may have adsorbed to the surface of the silica NPs, thereby increasing its size. This is also supported by examining the particles' morphology using a TEM (Figure 5.2). While the central particle is not significantly different from the original NPs, the addition of very small (1-3nm) denser particles seem to increase their

effective size and hydrodynamic diameter as measured by DLS. The zeta potential values showed minimal changes (data shown in Chapter III).

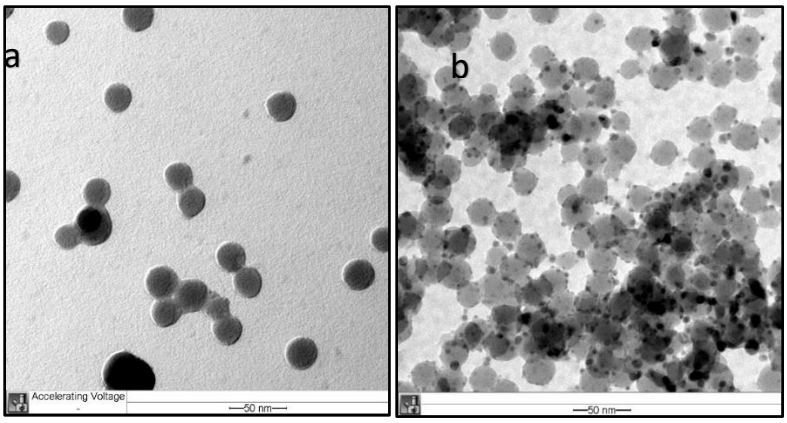

Figure 5.2 TEM Image of Slurry NPs (a) Before and (b) after CMP, 80,000x Magnification.

Table 5.1 Silica Dilution and Arsenic Concentration in Processed Slurry Samples.

Sample	Waste slurry dilution	Silica g/L	As µg/L	As/Si µg/g
3.5psi	4.1x	58.4	435.49	7.46
4.0psi	3.4x	69.7	451.60	6.48
5.0psi	3.8x	63.5	576.74	9.08
Dilute 5.0psi	7.2x	33.2	143.51	4.32
Dilute 9.0psi	3.9x	62.0	733.99	11.84
24h etch	1x	248	4798.57	19.35
72h etch	1x	248	12997.97	52.41

Gallium and Arsenic levels were evaluated for each sample. As part of sample preparation, slurry samples were filtered using 3 kDa centrifuge filter tubes (approx. 1 nm). Gallium was present in extremely low levels, so non-filtered samples were also analyzed for Ga and As content. Filter loss of Ga and As is interpreted to be removed particulate whereas the amount seen in both filtered and unfiltered samples represents the soluble forms of each element. On average, 94.5% of As was recovered from filtered CMP waste but less than 1% of Ga was recovered (data not shown). This is consistent with the formation of insoluble Ga_2O_3 particles following oxidation in water. [47] Silica levels were determined based on measured Si content to assess the precise dilution of each waste sample. Dilution of waste is variable due to the intermittent rinse cycle in the CMP tool, yielding 3.4-7.2x dilution factors. Due to this, As/Si ratio is as important as the final As concentration in the wastewater (Table 5.1). If there is no interaction in toxicity of As and SiO_2 NPs, then the As/Si ratio may dictate the primary toxicant.

V.3.4 Arsenic speciation

Arsenic species in the filtered samples were separated by HPLC and detected using ICP-MS. The method detected no observable amount of organic arsenic in the form of DMA or MMA. For inorganic species, As(III) was present in higher levels than As(V) for most samples (Table 5.2 and Figure 5.3). Most notably, the only sample with a higher As(V) level was the dilute 5.0 psi process sample, which also had the least amount of total As of all samples as well as the highest dilution factor. It is likely that the added water and native slurry oxidizers were enough to oxidize the small amount of As(III) to As(V) by the time the sample was tested 48hr after the CMP process. It is possible that

the amount of As(V) present in the other samples is also due to a slow natural oxidation of the Arsenic. The concentrated samples had a lower As(III)/As(V) ratio because speciation analysis was done days to weeks later. While the wet etched or dissolution samples (24hr ,72hr) were tested immediately after separation. For comparison, a 1-year old 5.0 psi slurry waste sample was also tested and had about 87% As(V) compared to As(III), validating the assumption that As(III) over time may oxidize to As(V). More studies are required on the auto-oxidation of slurry waste. Similarly, variable pH is believed to play a role in the oxidation process. The sample with the highest As levels (dilute 9.0 psi) was pH adjusted to pH of 3 to 11 for 24 hours before speciation analysis (Figure 5.4). Interestingly, no significant change in As(III)/As(V) ratio was observed. Additional studies are needed to determine if slurry composition is resulting in slow As(III) oxidation or As(V) reduction.

Table 5.2 As(III) and As(V) Levels for CMP Waste Samples.

Sample	As(III) µg/L	As(V) µg/L	As(III)/As(V) ratio
3.5psi	288.87	161.96	1.78
4.0psi	307.87	223.73	1.38
5.0psi	299.99	361.45	0.83
Dilute 5.0psi	10.94	136.36	0.08
Dilute 9.0psi	673.02	110.23	6.11
24h etch	4041.03	536.86	7.53
72h etch	11432.48	1575.83	7.25

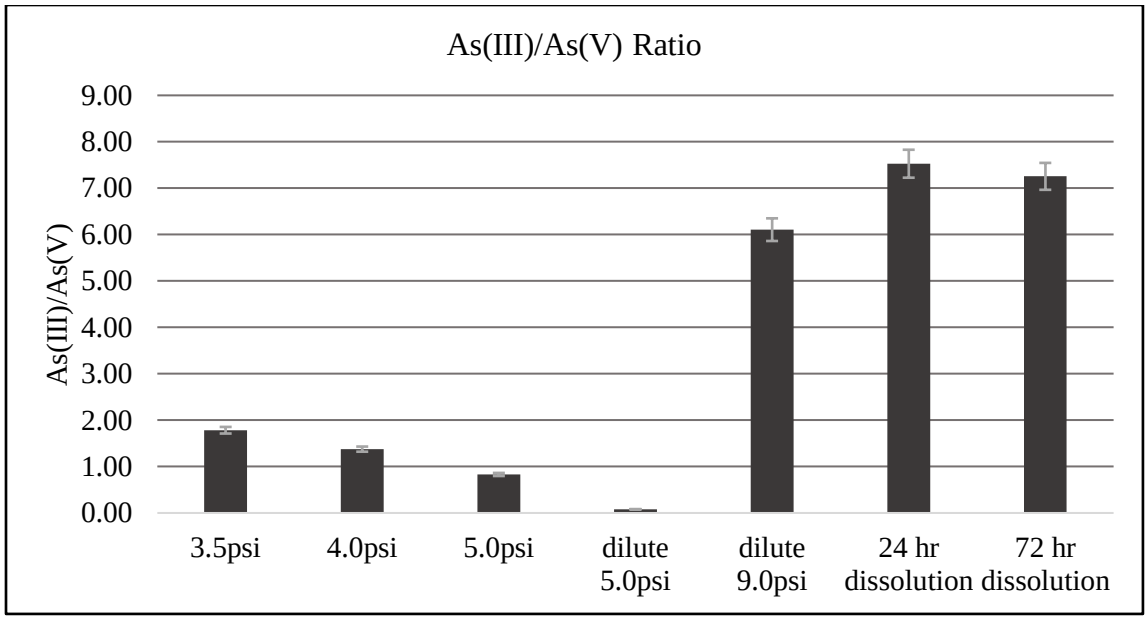

Figure 5.3 Arsenic Species Ratio for CMP Waste and Wet Etch Samples.

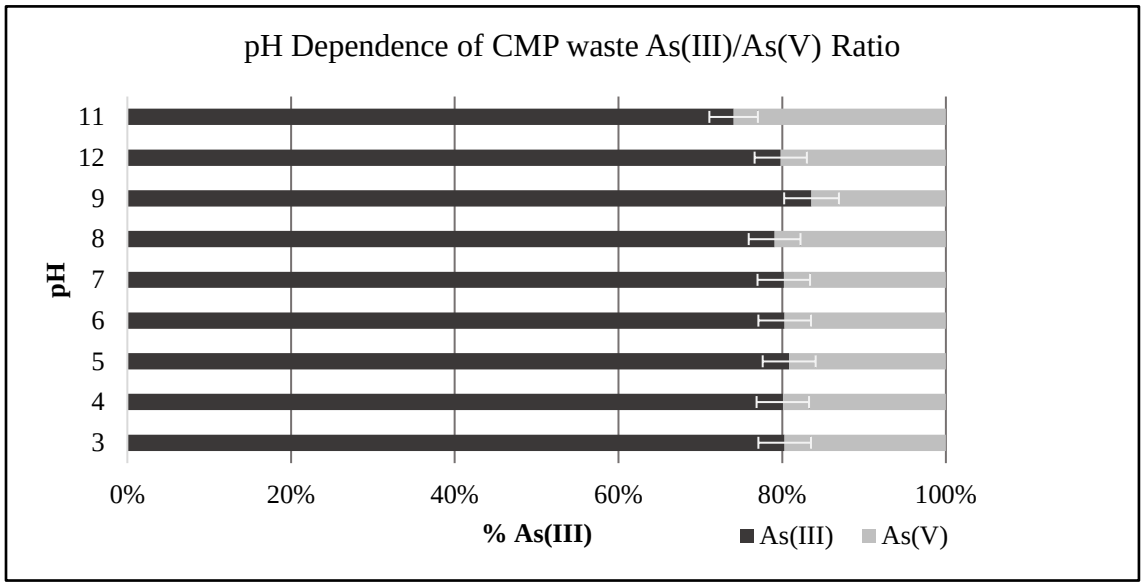

Figure 5.4 Arsenic Speciation Following pH Adjustment of Dilute 9.0 psi CMP Waste Sample. Sample is pH 9.0 at collection.

V.2.5 Cytotoxicity assays

To best assess the influence of arsenic on slurry toxicity, the sample with the highest As levels (dilute 9.0 psi) was used in vitro toxicity studies. Since the organ lining (epithelial) cells are the first to interact with toxicants or NPs that may enter the body, lung A549 cells were used. Overall, cell viability showed a strong dose-dependent response that showed no difference between stock slurry and used CMP waste (Figure 5a). Arsenic standards run concurrently showed an IC_{50} of 1.4 mg/L for As(III) and >10 mg/L for As(V). A substantial increase in apoptosis (programmed cell death) was also not detected in any samples despite a clear loss in viability, suggesting necrosis may be the primary mode of cell death. Membrane damage was measured by LDH release, an indication of necrotic cell death due to leaking of cellular contents. This showed a strong dose-dependent response with no difference between stock and CMP waste slurry (Figure 5.5).

Evaluated together, these studies indicate that the slurry NPs cause necrosis in a dose-dependent matter with an IC_{50} of approximately 300 mg/L SiO_2 with no observed toxicity contribution from the arsenic content in the post-CMP slurry. This slurry diluted to 300 mg/L SiO_2 would have an arsenic concentration of approximately 3.55 µg/L, well below the 10 µg/L maximum contaminant level (MCL) of arsenic in drinking water set by the EPA and only 0.25% of the IC_{50} determined in this study but higher than the airborne OSHA PEL TWA of 0.01 µg/L for inorganic arsenic in general industry (action level 0.005 µg/L). Even if the waste arsenic was entirely As(III), it would require 4.7 mg/L As to equal the toxic effect of SiO_2 NPs assuming no other interaction. This

situation is not realistic in CMP effluents without some extreme waste concentrations. Due to these ratios, the overall As contribution to the waste is not considered especially harmful as it is generated. However, the concentration of As in soil or organisms in the waste stream can increase this hazard. Additionally, the silica nanoparticles may be removed but they may also settle out and accumulate depending on their particular treatment and environmental fate. This bioaccumulation of either the NPs or As would likely be more hazardous.

a

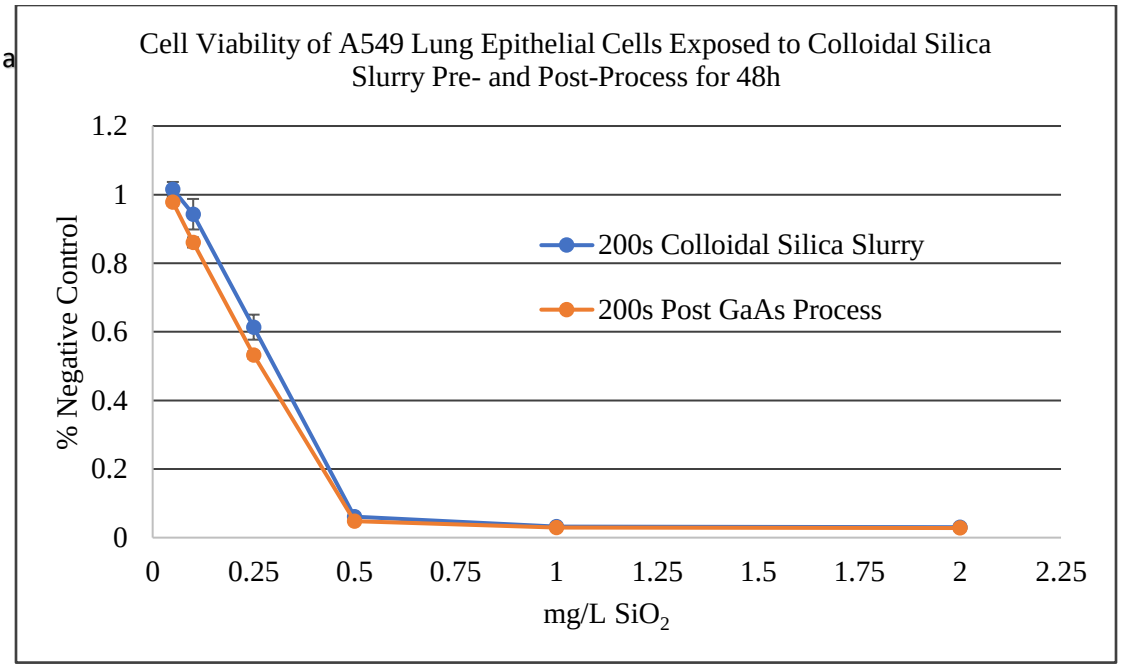

b

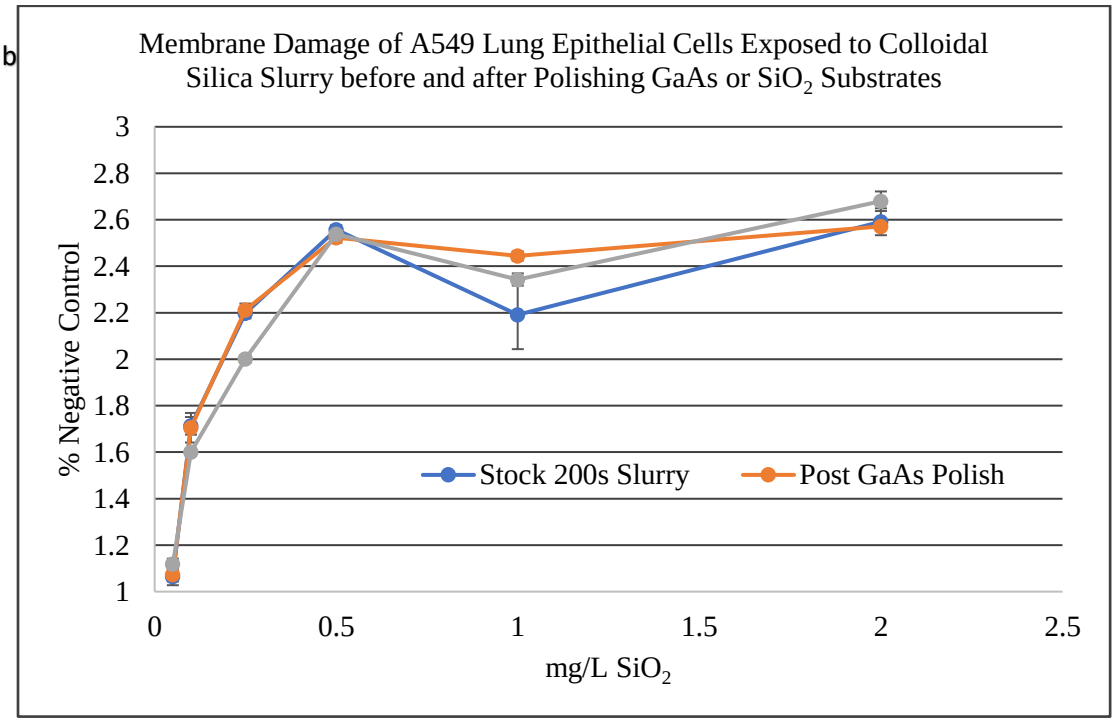

Figure 5.5 Viability (a) and Membrane Damage (b) of A549 Lung Epithelial Cells Exposed to Stock Slurry Containing Silica NPs and Wastewater from CMP of GaAs.

V.4 Conclusions

The prevalence of ENMs in consumer products and industrial processing will continue as the technology advances. As their use and manufacture increase, so too will the number of these materials entering the environment. Just like microplastics before them, the sheer number and miniscule size will allow this new class of material to completely permeate the air, water, and soil if not controlled. A major part of developing regulations and rules for the use or remediation of NPs is hazard identification. While existing literature establishes that NPs have size, shape, concentration and property-dependent toxicity, this variable toxicity can come from a single type of nanoparticle over its lifetime.

Just as consumer products age or wear, industrial NPs can have their properties modified in their normal/intended use. While ENMs can be transformed by other things once they enter the environment, some transformation can occur before they are ever sent to the landfill or dumped down the drain. Since property changes can cause a change in nano-bio interactions, this transformation can shift or even potentiate the toxicity in some types of nanoparticles if the right conditions are met.

In this study, a wide selection of common CMP processes was performed with varied slurry nanoparticles and substrate materials. The physicochemical properties of these nanoparticles were quantified and compared for the pre-and post-polish slurries and minor transformation of properties was discovered. Modest increases in size, reductions to the surface charge, and a marked increase in substrate material concentrations were quantified, though direct imaging and surface spectroscopy did not yield any details on

the location or surface modification of these added components. The one exception was small, 2-3nm particles hypothesized to be insoluble Ga in the colloidal silica slurry used to polish a GaAs wafer. Future work into the actual surface modifications and prevalence of foreign material impregnated into the NP surface would significantly improve this study. Single particle ICP-MS as well as precise auger or ISS analysis may also allow for the direct spectroscopic probing the nanoparticle surface more precisely than the penetrating XPS and EDX techniques.

In exploring the GaAs process specifically, it was discovered that the As entering the solution split between the more toxic As(III) and less toxic As(V) species, often favoring the former. This balance did not appear to be pH dependent over short time periods but was affected somewhat in an unquantified manner by changing CMP process conditions. Meanwhile, the Ga component was easily removed by ultrafine filtration. Despite the increased toxicity of As(III), the relative amount of As content to SiO_2 NPs was so low (µg/kg) that the particle toxicity overrode the As toxicity at all conditions.

For the other slurry samples, general toxicity in the form of metabolic activity and necrosis did not increase from the pre-process baselines. Apoptosis saw a slight, but significant, increase for most processes due to an unknown mechanism that is hypothesized to stem from the trace amounts of substrate material that aggregate around the nanoparticles, which may be brought to the cells by those NPs. ROS was increased by the As and Cu content, likely due to their classic (known) toxicity and ROS generating mechanisms. Future work should examine the specific radicals formed in these cells to elucidate a mechanism. Similarly, specific apoptosis pathways can be probed using

various biomarkers to narrow down the toxic mechanism of the post-process slurries. Exploring the leads exposed in this study may lead to divergent pathways due to the differing materials or operate on the same pathway due to physical similarities.

Significantly more work is needed to fully validate the role of processing-dependent nanoparticle transformation and correlate toxicity changes, but this study serves as a first step and proof of concept. Although minor, nanoparticle transformation did occur. It is not unreasonable to expect stronger transformation results from other processes now or in the future; in CMP or countless related mechanisms. Even these small changes did have a limited effect on toxicity in the form of cell death and oxidative stress and other interactions could be probed. For the smallest nanoparticles, colocalization using hyperspectral microscopy or other techniques can help identify changes. In the more general matter of hazard identification for risk assessment and the pursuit of "green" industry practices, this study has shown that nanoparticle transformation does happen due to processing and it does matter for toxicology assessment. This and related works may help to influence the various stakeholders and decisionmakers so that industry eventually looks at their nanomaterials from an end-of life perspective and not just the toxic effects of the off-the-shelf product.

CHAPTER VI

CONCLUSION AND FUTURE PERSPECTIVES

In conclusion, process effluent from chemical mechanical planarization was generated and studied for any nanoparticle transformation and resulting toxicity. An array of CMP processes were performed to represent the physicochemical breadth of the polishing done in industry with alumina, ceria, and various silica slurries used to polish SiO_2 films, copper films, and GaAs substrates. The collected waste samples were characterized for size, shape, surface charge, surface chemistry, and chemical bonding to compare any differences between pristine and waste samples.

Minor increases in hydrodynamic diameter and changes to surface charge were not apparent in TEM images or further chemical testing. It is most likely that the removed substrate material loosely bound or aggregated around the nanoparticles and were removed during the drying process or are present at a diminished ratio to the total number of nanoparticles. The silica polish of GaAs process demonstrated this best with visible 1-3nm nanoparticles in the TEM images that were determined to be insoluble Ga particles by filtration and ICP analysis. Added copper was also detected in those processes that polished copper films; enhanced Cu levels were detected by ICP but were most likely present primarily in an ionic or solubilized form that did not associate with the nanoparticles as it could only be partially filtered out as the Ga and main nanoparticles had been. No Cu particles were detected, so it is likely that the 30-50% that

was filtered out associated with the nanoparticles. Additionally, it was conclusively shown that the 30nm SiO_2 in particular increased in size after CMP processing but did not do so after having a GaAs coupon soak in a volume of the slurry for extended periods of time.

The GaAs polish process also had special considerations. The addition of gallium was characterized and identified by TEM and ICP analysis, and the arsenic appeared in a soluble form that did not associate so strongly with the silica nanoparticles that it could be captured by a filter. This arsenic was determined to be almost entirely inorganic species, predominantly as As(III), though the exact ratio of As III/V species appeared to be process dependent but not pH dependent in the short term. This speciation is important for the waste processing done to GaAs CMP effluent due to different treatment regimens for the arsenic chemical species. Arsine gas was not generated in a detectable concentration within the CMP.

The cytotoxicity of the slurry nanoparticles increased in a dose-dependent manner. The slurry nanoparticles required relatively high concentrations to elicit a toxic effect, with the lowest IC_{50} value above 250 mg/L. The intent of this study was to identify and research a shift in biological effect due to nanoparticle transformation. Waste slurry did not have a significant difference in viability or membrane damage compared to the pristine form. Apoptosis rates were significantly different for many waste samples but increased or decreased with no discernable pattern. The production of reactive oxygen species was higher from the polish of copper by alumina due to the increased copper content. The ROS generation by ceria nanoparticles after SiO_2 polish

decreased for liver and macrophage cells. This is likely due to the substrate material covering the ceria nanoparticles and preventing the chemical interactions creating the ROS in cells, though this should be verified through additional targeted testing. The viability, membrane damage, and oxidative stress results are straightforward and explainable, but the apoptosis data requires further investigation.

The apoptosis activity from all cell lines and most waste samples were significantly different from the new slurry without an apparent pattern. With no trend to follow and so many different nanoparticle types, it is difficult to develop a new hypothesis for this data without further study. Apoptosis is caused by a few major pathways and future work should first identify which of the major pathways each slurry combination is activating. Once the pathway is identified, individual biomolecule targets can be probed to discover the pathway modification or influence. Due to the disparity in results, it is likely that multiple pathways are activated in different cell lines or nanoparticle chemistries. It is probable that nanoparticle waste that decreases apoptosis rates is having its surface obfuscated by substrate material and the nano-bio interactions causing apoptosis are therefore decreasing. Increases in apoptosis may be due to the potentiation or synergistic effects of additional substrate material on a nanoparticle, increasing its reactivity with cellular machinery.

Another continuation of this work requires increasing the likelihood for nanoparticle transformation. The potential for transformation may be increased or transformed nanoparticles concentrated by continuously recirculating used slurry while processing or pursuing more extreme CMP process parameters. By increasing the degree

of transformation or number of affected particles, the identification of physicochemical change and the resulting biological effect will become more apparent. This may cause additional transformation as well as increase the existing effects that may be difficult to detect.

This research has taken a first step in identifying and characterizing nanoparticle transformation due to CMP processing. These changes created minor shifts in cytotoxicity and identified specific hazards or waste-related concerns. More work needs to be done to further examine the degree of transformation possible from industrial processing and how this might affect biological interactions. What has been shown in this document suggests that additional research into this transformation and the assessment of waste toxicity is a worthwhile exercise for scientific research and industry regulation.

REFERENCES

1. BCC (2007). Nanostructured Materials: Electronic/Magnetic/Optoelectronic. BCC Reports.

2. Belongia, B. M. (1999). Treatment of Alumina and Silica Chemical Mechanical Polishing Waste by Electrodecantation and Electrocoagulation. J. Electrochem. Soc. Journal of The Electrochemical Society **146**(11): 4124.

3. Bi, X. and P. Westerhoff (2016). Adsorption of III/V ions (In(III), Ga(III) and As(V)) onto SiO2, CeO2 and Al2O3 nanoparticles used in the semiconductor industry Electronic supplementary information (ESI) available. See DOI: 10.1039/c6en00184j. EN Environmental Science: Nano **3**(5): 1014-1026.

4. Brenner, S., Neu-Baker, N., Eastlake, A., Beaucham, C., & Geraci, C. (2016). NIOSH field studies team assessment: Worker exposure to aerosolized metal oxide nanoparticles in a semiconductor fabrication facility. Journal of Occupational and Environmental Hygiene **13**(11): 871.

5. Brenner, S., Neu-Baker, N., Caglayan, C., & Zurbenko, I. (2015). Occupational Exposure to Airborne Nanomaterials: An Assessment of Worker Exposure to Aerosolized Metal Oxide Nanoparticles in Semiconductor Wastewater Treatment. Journal of Occupational and Environmental Hygiene 12:7 469-481.

6. Choi, K., Kim, J., Park, J., Kim, K., & Bae, G. (2015). Exposure Characteristics of Nanoparticles as Process By-products for the Semiconductor Manufacturing Industry. Journal of Occupational and Environmental Hygiene **12**(8): 153-160.

7. Corlett, G. (2000). Targeting water use at chemical mechanical polishing. SOLID STATE TECHNOLOGY **43**: 201-208.

8. Crawford, S. and S. Aravamudhan (2017). Environmental Impact and Speciation Analysis of Chemical Mechanical Planarization (CMP) Waste Following GaAs Polishing. ECS Transactions **80**(2): 171-179.

9. De Luna, M., W., & Liu, J. (2009). Combined treatment of polishing wastewater and fluoride-containing wastewater from a semiconductor manufacturer. COLSUA Colloids and Surfaces A: Physicochemical and Engineering Aspects **347**(1-3): 64-68.

10. Dive, C., Gregory, C., Phipps, D., Evans, D., Milner, A., & Wyllie, A. (1992). Analysis and discrimination of necrosis and apoptosis (programmed cell death) by multiparameter flow cytometry. BBAMCR BBA - Molecular Cell Research **1133**(3): 275-285.

11. Dumitrescu, E., Karunaratne, D., Babu, S., Wallace, K., & Andreescu, S. (2018). Interaction, transformation and toxicity assessment of particles and additives used in the semiconducting industry. CHEM Chemosphere **192**: 178-185.

12. Egger, A., Rappel, C., Jakupec, M., Hartinger, C., Heffeter, P., & Keppler, B. (2009). Development of an experimental protocol for uptake studies of metal compounds in adherent tumor cells. Journal of analytical atomic spectrometry **24**(1): 51-61.

13. El Badawy, A., Silva, R., Morris, B., Scheckel, K., Suidan, M., & Tolaymat, T. (2011). Surface Charge-Dependent Toxicity of Silver Nanoparticles. Environmental Science & Technology **45**(1): 283.

14. Fent, K., Weisbrod, C., Wirth-Heller, A., & Pieles, U. (2010). Assessment of uptake and toxicity of fluorescent silica nanoparticles in zebrafish *Danio rerio* early life stages. AQTOX Aquatic Toxicology **100**(2): 218-228.

15. Oberdörster, G., Andrew, M., Ken, D., Vincent, C., Julie, F., Kevin, A., . . . Hong, Y. (2005). Principles for characterizing the potential human health effects from exposure to nanomaterials: elements of a screening strategy. Particle and Fibre Toxicology **2**: 8.

16. Zhang, H., Dunphy, D., Jiang, X., Meng, H., Sun, B., Tarn, D., . . . Brinker, C. (2012). Processing pathway dependence of amorphous silica nanoparticle toxicity: Colloidal vs pyrolytic. Journal of the American Chemical Society, 134(38), 15790-804.

17. Karlsson, H., Gustafsson, J., Cronholm, P., & Möller, L. (2009). Size-dependent toxicity of metal oxide particles--a comparison between nano- and micrometer size. Toxicology letters **188**(2): 112-118.

18. Kosaraju, K., Crawford, S., & Aravamudhan, S. (2015). Cellular Toxicity Assessment and Environmental Impact of Pre- and Post-CMP Nanoparticle Slurries. ECS Transactions ECS Transactions **69**(40): 1-5.

19. Kosaraju, K., Crawford, S., Tarannum, M., & Aravamudhan, S. (2015). Assessment of Change in Physicochemical Properties and Cellular Toxicity of Pre- and Post-CMP Silica Slurries. ECS J. Solid State Sci. Technol. ECS Journal of Solid State Science and Technology **4**(11): P5068-P5072.

20. Kosaraju, K., Tarannum, M., Crawford, S., Garde, K., & Aravamudhan, S. (2014). Examining the Cellular Uptake and Toxicity of Engineered Nanomaterials. ECS Transactions **61**(36): 15-21.

21. Krishnan, M., Nalaskowski, J., & Cook, L. (2010). Chemical Mechanical Planarization: Slurry Chemistry, Materials, and Mechanisms. Chemical Reviews **110**(1): 178-204.

22. Lin, S. H. and Yang, C.R. (2004). Chemical and physical treatments of chemical mechanical polishing wastewater from semiconductor fabrication. Journal of Hazardous Materials **108**(1): 103-109.

23. Lin, W., Huang, Y., Zhou, X., & Ma, Y. (2006). In vitro toxicity of silica nanoparticles in human lung cancer cells. YTAAP Toxicology and Applied Pharmacology **217**(3): 252-259.

24. Liu, X. and K. L. Chen (2016). Aggregation and interactions of chemical mechanical planarization nanoparticles with model biological membranes: role of phosphate adsorption. Environ. Sci.: Nano Environ. Sci.: Nano **3**(1): 146-156.

25. Moore, M. N. (2006). Do nanoparticles present ecotoxicological risks for the health of the aquatic environment? EI Environment International **32**(8): 967-976.

26. Nel, A., Madler, L., & Li, N. (2006). Toxic Potential of Materials at the Nanolevel. Science **311**(5761): 622-627.

27. Peña, M., Gottipati, A., Tahiliani, S., Neu-Baker, N., Frame, M., Friedman, A., & Brenner, S. (2016). Hyperspectral imaging of nanoparticles in biological samples: Simultaneous visualization and elemental identification. JEMT Microscopy Research and Technique **79**(5): 349-358.

28. Riss, T., Hook, B., & Duellman, S. (2015). Evaluation of real time cell viability assays multiplexed with other methods. Toxicology Letters Toxicology Letters **238**(2): S179-S180.

29. Seung, W., In, H., & Soong, H. (2015). Role of Physicochemical Properties in Nanoparticle Toxicity. Nanomaterials (2079-4991) **5**(3).

30. Jia, X., Di, Y., Feng, J., Yang, Q., Dai, H., & Lee, J. (February 01, 2018). Adaptive virtual metrology for semiconductor chemical mechanical planarization process using GMDH-type polynomial neural networks. Journal of Process Control, 62, 44-54

31. Speed, D., Westerhoff, P., Sierra-Alvarez, R., Draper, R., Pantano, P., Aravamudhan, S., . . . Shadman, F. (2015). Physical, chemical, and in vitro toxicological characterization of nanoparticles in chemical mechanical planarization suspensions used in the semiconductor industry: towards environmental health and safety assessments. Environ. Sci.: Nano Environ. Sci.: Nano **2**(3): 227-244.

32. Srinivas, A., Rao, P., Selvam, G., Murthy, P., & Reddy, P. (2011). Acute inhalation toxicity of cerium oxide nanoparticles in rats. TOXLET Toxicology Letters **205**(2): 105-115.

33. Stoeger, T., Takenaka, S., Frankenberger, B., Ritter, B., Karg, E., Maier, K., . . . Schmid, O. (2009). Deducing in Vivo Toxicity of Combustion-Derived Nanoparticles from a Cell-Free Oxidative Potency Assay and Metabolic Activation of Organic Compounds. Environmental Health Perspectives **117**(1): 54-60.

34. Waters, K., Masiello, L., Zangar, R., Tarasevich, B., Karin, N., Quesenberry, R., . . . Thrall, B. (2009). Macrophage Responses to Silica Nanoparticles are Highly Conserved Across Particle Sizes. Toxicological Sciences **107**(2): 553-569.

35. Westerhoff, P., Kiser, M., & Hristovski, K. (2013). Nanomaterial removal and transformation during biological wastewater treatment. Environ. Eng. Sci. Environmental Engineering Science **30**(3): 109-117.

36. Xia, T., Kovochich, M., Liong, M., Mädler, L., Gilbert, B., Shi, H., . . . Nel, A. (2008). Comparison of the mechanism of toxicity of zinc oxide and cerium oxide nanoparticles based on dissolution and oxidative stress properties. ACS nano **2**(10): 2121-2134.

37. Yang, G. C. C. (2002). CMP wastewater management using the concepts of design for environment. EP Environmental Progress **21**(1): 57-62.

38. Zantye, P., Kumar, A., & Sikder, A. (2004). Chemical mechanical planarization for microelectronics applications. MSR Materials Science & Engineering R **45**(3): 89-220.

39. Del Alamo JA. (2011). Nanometre-Scale Electronics with III-V Compound Semiconductors. Nature, 479(7373): 317–23.

40. Heyns, M., & Tsai, W. (2009). Ultimate scaling of cmos logic devices with Ge and III–V materials. MRS Bulletin, 34(07), 485-492.

41. Holden, P., Klaessig, F., Turco, R., Priester, J., Rico, C., Avila-Arias, H., Gardea-Torresdey, J. (2014). Evaluation of exposure concentrations used in assessing manufactured nanomaterial environmental hazards: Are they relevant? Environmental Science & Technology, *48*(18), 10541-10541.

42. Roth, G., Neu-Baker, N., & Brenner, S. (2015). Sem analysis of particle size during conventional treatment of cmp process wastewater. The Science of the Total Environment, 508, 1-6.

43. Karimi, S., Troeung, M., Wang, R., Draper, R., Pantano, P., Crawford, S., & Aravamudhan, S. (2019). Acute and chronic toxicity to daphnia magna of colloidal silica nanoparticles in a chemical mechanical planarization slurry after polishing a gallium arsenide wafer. Nanoimpact, 13, 56-65.

44. Torrance, K., Keenan, H., Hursthouse, A., & Stirling, D. (2010). Measurement of arsenic and gallium content of gallium arsenide semiconductor waste streams by icp-ms. Journal of Environmental Science and Health. Part A, Toxic/hazardous Substances & Environmental Engineering,45(4), 471-471.

45. R mili, B., Le Bihan, O., Dutouquet, C., Aguerre-Charriol, O., & Frejafon, E. (2013). Particle sampling by tem grid filtration. Aerosol Science and Technology, 47(7), 767-775.

46. Baun, A., Hartmann, N., Grieger, K., & Kusk, K. (2008). Ecotoxicity of engineered nanoparticles to aquatic invertebrates: A brief review and recommendations for future toxicity testing. Ecotoxicology, 17(5), 387-395.

47. Matovu, J., Ong, P., Leunissen, L., Krishnan, S., & Babu, S. (2013). Fundamental investigation of chemical mechanical polishing of gaas in silica dispersions: Material removal and arsenic trihydride formation pathways. ECS Journal of Solid State Science and Technology, 2(11), 439.

48. Peters, T., Elzey, S., Johnson, R., Park, H., Grassian, V., Maher, T., & O'Shaughnessy, P. (2008). Airborne monitoring to distinguish engineered nanomaterials from incidental particles for environmental health and safety. Journal of Occupational and Environmental Hygiene, 6(2), 73-81.

49. Vetten, M., Tlotleng, N., Tanner Rascher, D., Skepu, A., Keter, F., Boodhia, K., Gulumian, M. (2013). Label-free in vitro toxicity and uptake assessment of citrate stabilised gold nanoparticles in three cell lines. Particle and Fibre Toxicology, 10(1), 50-50. doi:10.1186/1743-8977-10-50

50. Nowack, B., Ranville, J. F., Diamond, S., Gallego-Urrea, J. A., Metcalfe, C., Rose, J., Horne, N., Koelmans, A. A., and Klaine, S.J. (2012). Potential scenarios for nanomaterial release and subsequent alteration in the environment. Environ. Toxicol. Chem., 31, 50–59.

51. Wiesner MR, Lowry GV, Alvarez P, Dionysiou D, Biswas P. 2006. Assessing the risks of manufactured nanomaterials. Environ Sci Technol 40:4336–4345

52. Lowry, G. V., Gregory, K. B., Apte, S. C., and Lead, J. R. (2012). Transformations of nanoparticles in the environment. Environ. Sci. Technol., 46, 6893–6899.

53. Lei, C., Sun, Y., Tsang, D. C. W., & Lin, D. (January 01, 2018). Environmental transformations and ecological effects of iron-based nanoparticles. Environmental Pollution, 232, 10-30.

54. Masciangioli, T. M., Alper, J., & National Research Council (U.S.). (2012). Challenges in Characterizing Small Particles: Exploring particles from the nano- to microscale: a workshop summary. Washington, D.C: National Academies Press.

55. Gwinn MR, Vallyathan V (2006) Nanoparticles: Health Effects-Pros and Cons. Environmental Health Perspectives 114(12) 1818-1825.

56. Roco, M. (2011). The long view of nanotechnology development: The national nanotechnology initiative at 10 years. Journal of Nanoparticle Research : An Interdisciplinary Forum for Nanoscale Science and Technology, 13(3), 1335-1335.

57. Keller, A., McFerran, S., Lazareva, A., & Suh, S. (2013). Global life cycle releases of engineered nanomaterials. Journal of Nanoparticle Research : An Interdisciplinary Forum for Nanoscale Science and Technology,15(6), 1-17. doi:10.1007/s11051-013-1692-4

58. Davis, G. (1986). The pathogenesis of silicosis. state of the art. Chest, 89(3), 166.

59. Castranova, V., Vallyathan, V., & Wallace, W. (1996). Silica and silica-induced lung diseases. Boca Raton: CRC Press.

60. Yu, K., Grabinski, C., Schrand, A., Murdock, R., Wang, W., Gu, B., . . . Hussain, S. (2009). Toxicity of amorphous silica nanoparticles in mouse keratinocytes. Journal of Nanoparticle Research, 11(1), 15-24. doi:10.1007/s11051-008-9417-9

61. Ye, Y., Liu, J., Chen, M., Sun, L., & Lan, M. (2010). In vitro toxicity of silica nanoparticles in myocardial cells. Environmental Toxicology and Pharmacology, 29(2), 131-137.

62. Malugin, A., Herd, H., & Ghandehari, H. (2011). Differential toxicity of amorphous silica nanoparticles toward phagocytic and epithelial cells. Journal of Nanoparticle Research, 13(10), 5381-5396.

63. Li, Y., Yu, Y., Duan, J., Yang, M., Wang, J., Jing, L., & Sun, Z. (2018). The internalization, distribution, and ultrastructure damage of silica nanoparticles in human hepatic l-02 cells. Nanomedicine: Nanotechnology, Biology and Medicine, 14(5), 1794-1794.

64. Pisani, C., Gaillard, J., Nouvel, V., Odorico, M., Armengaud, J., & Prat, O. (2015). High-throughput, quantitative assessment of the effects of low-dose silica nanoparticles on lung cells: Grasping complex toxicity with a great depth of field. Toxicology Letters, 238(2), 229.

65. Mannerström, M., Zou, J., Toimela, T., Pyykkö, I., & Heinonen, T. (2016). The applicability of conventional cytotoxicity assays to predict safety/toxicity of mesoporous silica nanoparticles, silver and gold nanoparticles and multi-walled carbon nanotubes. Toxicology in Vitro, 37, 113-120

66. Lesniak, A., Fenaroli, F., Monopoli, M., Åberg, C., Dawson, K., & Salvati, A. (2012). Effects of the presence or absence of a protein corona on silica nanoparticle uptake and impact on cells. ACS Nano, 6(7), 5845-5857.

67. Wang, F., Gao, F., Lan, M., Yuan, H., Huang, Y., & Liu, J. (2009). Oxidative stress contributes to silica nanoparticle-induced cytotoxicity in human embryonic kidney cells. Toxicology in Vitro, 23(5), 808-815.

68. Duan, J., Yu, Y., Li, Y., Zhou, X., Huang, P., & Sun, Z. (2013). Toxic effect of silica nanoparticles on endothelial cells through dna damage response via chk1-dependent g2/m checkpoint. Plos One, 8(4), 62087.

69. Donaldson, K., Brown, D., Clouter, A., Duffin, R., MacNee, W., Renwick, L., . . . Stone, V. (2002). The pulmonary toxicology of ultrafine particles. Journal of Aerosol Medicine, 15(2), 213-220

70. Irfan, A., Cauchi, M., Edmands, W., Gooderham, N., Njuguna, J., & Zhu, H. (2014). Assessment of temporal dose-toxicity relationship of fumed silica nanoparticle in human lung a549 cells by conventional cytotoxicity and ^{1}h-nmr-based extracellular metabonomic assays. Toxicological Sciences, 138(2), 354-364.

71. Flaherty, N., Chandrasekaran, A., Peña, M., Roth, G., Brenner, S., Begley, T., & Melendez, J. (2015). Comparative analysis of redox and inflammatory properties of pristine nanomaterials and commonly used semiconductor manufacturing nano-abrasives. Toxicology Letters, 239(3), 205-215.

72. Geiser, M., Rothen-Rutishauser, B., Kapp, N., Schürch, S., Kreyling, W., Schulz, H., . . . Gehr, P. (2005). Ultrafine particles cross cellular membranes by nonphagocytic mechanisms in lungs and in cultured cells. Environmental Health Perspectives, 113(11), 1555-1560.

73. Chang, K. (2007). In vitro cytotoxicitiy of silica nanoparticles at high concentrations strongly depends on the metabolic activity type of the cell line. Environmental Science & Technology, 41(6), 2064-2064.

74. Barnes, C., Elsaesser, A., Arkusz, J., Smok, A., Palus, J., Leśniak, A., . . . Howard, C. (2008). Reproducible comet assay of amorphous silica nanoparticles detects no genotoxicity. Nano Letters, 8(9), 3069-74.

75. Hamilton, R., Thakur, S., & Holian, A. (2008). Silica binding and toxicity in alveolar macrophages. Free Radical Biology & Medicine, 44(7), 1246-58.

76. Bandyopadhyay, A., Das, T., & Yeasmin, S. (2014). Nanoparticles in lung cancer therapy - recent trends (Springerbriefs in molecular science). New Delhi: Springer. (2014)

77. Vivero-Escoto, J. (2012). Silica nanoparticles : Preparation, properties, and uses (Nanaotechnology science and technology). New York: Nova Science. (2012)

APPENDIX A

CMP PROCESS PARAMETERS

Slurry	Substrate	Time mm:ss	Platen Speed (rpm)	Carrier Speed (rpm)	Down Force (psi)	Back Pressure (psi)	Substrate size (mm)
Alumina (A20)	Copper	2:00	30	36	10.0	2.0	200
Ceria (CES 333)	SiO2	2:00	60	72	12.0	2.0	200
Colloidal Silica (200s)	SiO2	2:30	60	72	5.0	1.5	200
Colloidal Silica (200x)	GaAs	1:30	60	72	3.5-9.0	1.5	150
Colloidal Silica (ACuPLANE)	Copper	2:00	48	60	12.0	2.0	200
Fumed Silica (12E)	SiO2	5:00	60	72	6.0	1.5	200

CMP process settings for main polish step on Avanti 472 Tool